Development of a Cost-Effective 1.5kN Liquid-Fueled Rocket Propulsion System

Jason Chen [*1], Srikar Gouru [†2], Sophia Troshynski [‡3], Ron Nachum [§4], Ankit Khandelwal [¶5], Ethan Ai [‖6], and Dabini Muldoon [**7]

[1] *Project Lead and Chief Engineer,* [2] *Flight and Ground Software Lead,* [3] *Manufacturing Lead,* [4] *Propulsion Lead,* [5] *Avionics Lead,* [6] *CAD and Testing Lead,* [7] *Structures and Ground Operations Lead*

Project Caelus, 501(c)(3)
(Initial revision 06 August, 2019; final revision 06 April, 2020)

The design of the propulsion system for a liquid-propellant sounding rocket, named Callisto 1, is presented. This propulsion system, named Aphlex 1B, has a nominal thrust of 1500 N and a total impulse of 6140 Ns. Aphlex 1B is designed to propel Callisto 1 to 1500 m altitude (5000 ft) on a payload mass of around 2 kg (4.4 lbm). Aphlex 1B is designed to be as simple and cost-effective as possible, due to financial constraints. Aphlex 1B's plumbing system is being extensively tested through a series of cold flow tests before progressing to static hot fire testing to evaluate flight-worthiness. During engine tests and test flights, the rocket will remain in constant communication with a ground station to relay telemetry and respond to commands, although the majority of flight events will be automatically controlled by an on-board commercial flight computer. The rocket's primary objective is to reach the target altitude and be recovered safely, and therefore, the payload has not yet been determined. The first cold flow test is due before 01 June, 2020 and the first static fire test is projected for 01 December, 2020. The inaugural flight of Callisto 1 is set for 01 June, 2021.

[*]jay.chen135@gmail.com, contact@projectcaelus.org
[†]srikarg89@gmail.com
[‡]stroshynski@gmail.com
[§]ronnachum13@gmail.com
[¶]amtron521@gmail.com
[‖]ethanai22@gmail.com
[**]cdabinim2249@gmail.com

Nomenclature

Symbols				**Acronyms**		
ϵ	=	Expansion ratio		CEA	=	Chemical equilibrium
γ	=	Ratio of specific heats				with applications
ρ	=	Density	g/cm^3	$COTS$	=	Commercial off-the-shelf
C^*	=	Characteristic velocity	m/s	DAQ	=	Data acquisition & control
C_d	=	Discharge coefficient		FOD	=	Foreign object debris
C_v	=	Valve flow coefficient		$GLOW$	=	Gross lift-off weight
f_d	=	Friction factor		$MECO$	=	Main engine cut-off
F_t	=	Thrust	N	MPV	=	Main propellant valve
g_0	=	Acceleration due to gravity	m/s^2	$P\&ID$	=	Piping and
I_{sp}	=	Specific impulse	s			instrumentation diagram
$\dot{m}$	=	Mass flow rate	kg/s	PT	=	Pressure transducer
O/F	=	Oxidizer-to-fuel ratio		TC	=	Thermocouple
Q	=	Volumetric flow rate	L/s	SF	=	Safety factor

Note: Subscripts follow the convention outlined in [3]. Unless otherwise specified, subscript 0 indicates at stagnation or impact conditions, 1 indicates conditions at the nozzle inlet or combustion chamber, t indicates the nozzle throat, 2 is at the nozzle exit, and 3 is at ambient conditions.

1 Introduction

Project Caelus is a 501(c)(3) non-profit organization consisting entirely of high school students from the northern Virginia area with a mission to design, build, and fly a liquid-propellant rocket to the Karman line by 2025. *Callisto 1*, the first of three experimental sounding rockets projected for completion by Project Caelus, has a target altitude of 1.5 km and is a technology and mission demonstrator for the organization. Project Caelus will be one of the first high school organizations to ever attempt a liquid-propellant rocket launch. The organization was founded in November 2018 and has since accumulated a membership of 41 freshmen, sophomore, junior, and senior students. The team is organized into three subsystems: propulsion, software, and outreach. The propulsion team manages all engineering aspects of the rocket, including the design, production, and testing of the propulsion system, airframe, payload, and ground infrastructure. The software team manages avionics, startup and abort sequences, data acquisition, and communication systems. The outreach team manages finances and outreach campaigns for aerospace and STEM in the local community. Currently, Project Caelus is almost completely crowdfunded, with some assistance from cooperate sponsors. More information, including further mission details and testing information, can be found at `projectcaelus.org`.

2 Initial System Characterization

Project Caelus's unique circumstance as an organization consisting entirely of high school students has laid the foundation for a design approach fully committed to cost-effectiveness, simplicity, and reliability. The following section outlines the initial design choices made for the overall propulsion system and reflects the organization's emphasis on the aforementioned ideals.

2.1 Objectives

The Callisto 1 system is set to the following constraints and objectives:

1. Reach an altitude of 1500 m ($\approx$ 5000 ft).
2. A $GLOW$ of no more than 35 kg ($\approx$ 77 lbsm).
3. A nominal main engine thrust of 1.5 kN ($\approx$ 350 lbsf).
4. A chamber pressure in the range of around 15 Bar to 20 Bar ($\approx$ 218 psi to 300 psi)
5. A nominal burn time of around 5 seconds.
6. Consume a budget of no more than $50,000 USD.

7. Utilize 95% ethyl alcohol and nitrous oxide as the propellant combination.

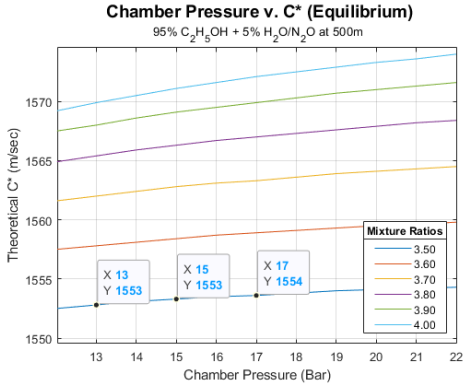

Figure 1: Theoretical C* efficiency vs chamber pressure and numerous mixture ratios.

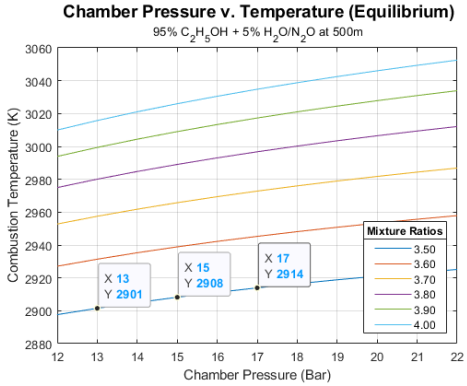

Figure 2: Combustion temperature vs chamber pressure and numerous mixture ratios.

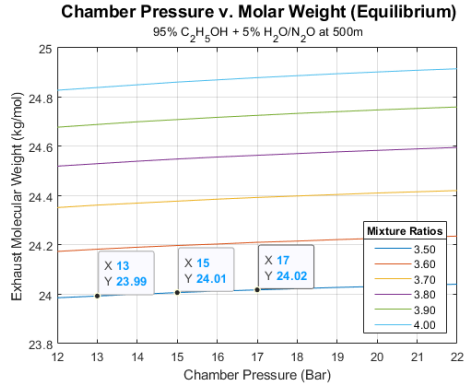

Figure 3: Gas molecular mass vs chamber pressure and numerous mixture ratios.

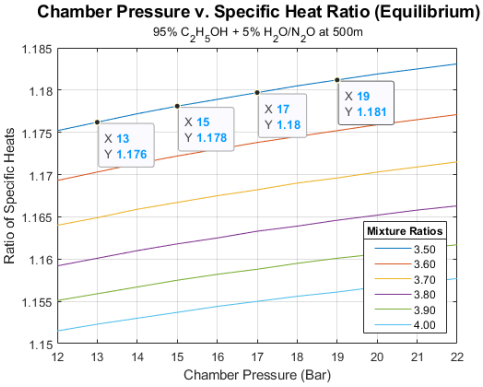

Figure 4: Ratio of specific heats vs chamber pressure and numerous mixture ratios.

2.2 Chamber Pressure and Mixture Ratio Selection

The first step is to realize the theoretical maximum performance to be expected from our propellant combination. 95% ethyl alcohol (ethanol) was chosen for its availability, low pricing, and a modest specific impulse. A 95% dilution (by mass) with water was chosen as to lower the expected combustion chamber temperature. This trade-off sacrifices some I_{sp} but reduces engineering complexity as regenerative and film cooling circuits may not be required. Industrial nitrous oxide was chosen as the main oxidizer for its self-pressurizing characteristics, non-cryogenic nature as opposed to liquid oxygen, relative ease to obtain, and a modest I_{sp} with ethanol. Using CEA, an open-source thermodynamics library provided by NASA's Glenn Research Center, critical data describing propellant combustion characteristics could be obtained. Numerical Python scripts were written to iterate through various combustion chamber pressures and mixture ratios and interface with CEA, and MATLAB scripts were used to parse and graph the CEA outputs as shown in Figures 1, 2, 3, and 4. Mixture ratios of 4.0 and 4.2 are labeled at certain chamber pressures. All dependent-variable properties (characteristic velocity C^*, combustion temperature T_c, exhaust molar mass M, and exhaust specific heat ratio γ) were permuted assuming shifting equilibrium flow and at an operational altitude of 500 m.

A mixture ratio of 4.0 was chosen for Aphlex 1B mainly in the interest of a conservative combustion temperature of around 3026 K and a middle-of-the-line theoretical C^* of around 1570 m/s, given a chamber pressure of 15 bar. This chamber pressure was chosen primarily in the interest of saving costs. A lower chamber pressure minimizes upstream fluid pressures and thus tank weight requirements, as well as requiring less expensive equipment that may otherwise be required. Although engine efficiency is sacrificed, this was not of primary concern. Preliminary literature reviews additionally showed that 15 bar (≈218 psi) was around the minimal operable chamber pressure, since a further decrease in chamber pressure would not allow critical pressure, a requirement for choked flow at the nozzle throat, to occur.

3 Engine System Design

The following section outlines the design process for Aphlex 1B, a second-generation bi-propellant liquid rocket engine, set to fly Callisto 1 given the objectives and data obtained in the previous section.

3.1 Nozzle Design

Design Parameters and Fluid Characteristics		
Name	Value	Unit
Propellant (Fuel)	Ethanol (C_2H_5OH, 95%)	N/A
Propellant (Oxidizer)	Nitrous oxide (N_2O)	N/A
O/F, Oxidizer/fuel ratio	4.0	N/A
F_t, Nominal thrust	1.50	kN
t_b, Burn time	5.0	sec
I_{total}, Total impulse	7500	$N * s$
P_c, Chamber static pressure	1.5×10^6	Pa
P_e, Ambient pressure	9.5540×10^4	Pa
T_c, Chamber static temperature	3025.98	K
M, Exhaust molecular mass	24.861	kg/mol
γ, Specific heat ratio	1.1537	N/A

Table 1: Summary of design parameters and fluid characteristics.

The nozzle design process followed standard procedures outlined in Rocket Propulsion Elements [3] and open-source NASA documents. The thermodynamic properties of the exhaust gas and other important parameters are summarized and compiled in Table 1. The ambient pressure was calculated using NASA Glenn Research Center's Earth Atmosphere Model for an altitude within the troposphere (less than 11000 meters), as shown in Equations 3.1 and 3.2, where T_3 represents the ambient temperature in Kelvin, h is the altitude in meters, P_3 is the ambient pressure in Pascals.

$$T_3 = 15.04 - 0.00649h \tag{3.1}$$

$$P_3 = \left[101.29 \times \left(\frac{T + 273.1}{288.08}\right)^{5.256}\right] \times 1000 \tag{3.2}$$

Assuming fully isentropic flow (by definition both adiabatic and reversible) in the supersonic nozzle with choked flow conditions at the throat, an ideal converging-diverging (de Laval) nozzle can be characterized. The first parameter to calculate is the controlling area ratio

$$\frac{A_t}{A_2} = \left(\frac{\gamma+1}{2}\right)^{1/(\gamma-1)} \left(\frac{p_2}{p_1}\right)^{1/\gamma} \sqrt{\frac{\gamma+1}{\gamma-1}\left[1 - \left(\frac{p_2}{p_1}\right)^{(\gamma-1)/\gamma}\right]} \tag{3.3}$$

where A_t is the cross-sectional area of the throat, A_2 is the cross-sectional area at nozzle exit, and p_1 and p_2 are the chamber pressure and exit pressure respectively. Equation 3.3 is also often referred to as the inverse of the expansion ratio ϵ, since $\epsilon = A_2/A_t$. Evaluating Equation 3.3 gives

$$\frac{A_t}{A_2} = \left(\frac{2.15}{2}\right)^{1/0.15} \left(\frac{9.6 \times 10^4}{1.5 \times 10^6}\right)^{1/1.15} \sqrt{\frac{2.15}{0.15}\left[1 - \left(\frac{9.6 \times 10^4}{1.5 \times 10^6}\right)^{0.15/1.15}\right]} = 0.307$$

Notice the substitution of p_2 for P_e as specified in Table 1, since in an ideal nozzle, the exhaust gas should expand to ambient pressure. The expansion ratio ϵ is simply

$$\epsilon = A_2/A_t = 1/AR = 1/0.307 = 3.26$$

Next, we can find the ideal exit velocity v_2, sometimes denoted as c:

$$v_2 = \sqrt{\frac{2\gamma}{\gamma-1}\left(\frac{R_u T_1}{M}\right)\left[1 - \left(\frac{p_2}{p_1}\right)^{(\gamma-1)/\gamma}\right]} \tag{3.4}$$

where R_u is the universal gas constant of 8314.3 J/kg mol-K and M is the molecular mass of the gas as shown in Table 1. Evaluating gives

$$v_2 = \sqrt{\frac{2 * 1.15}{0.15}\left(\frac{8314.3 * 3026}{24.86}\right)\left[1 - \left(\frac{9.6 \times 10^4}{1.5 \times 10^6}\right)^{0.15/1.15}\right]} = 2162.3\ m/s$$

Next, the mass flow rate $\dot{m}$ can be calculated explicitly noting that $v_2 = c$, since earlier it was stated that $p_2 = p_3$:

$$\dot{m} = F_t/c = 1500/2162.3 = 0.694\ kg/s \tag{3.5}$$

Solving using our chosen O/F ratio of 4.0 for each independent propellant $\dot{m}$ gives

$$\dot{m}_o = \dot{m} * (4/5) = 0.694 * (4/5) = 0.555\ kg/s$$
$$\dot{m}_f = \dot{m} * (1/5) = 0.694 * (1/5) = 0.139\ kg/s$$

Next, we arrive at the throat area:

$$A_t = \frac{\dot{m}}{p_1}\sqrt{\frac{(R_u/M)T_1}{\gamma[2/(\gamma+1)]^{(\gamma+1)/(\gamma-1)}}} \tag{3.6}$$

Evaluating Equation 3.6 gives

$$A_t = \frac{0.694}{1.5 \times 10^6}\sqrt{\frac{(8314.3/24.86) * 3026}{1.15[2/(2.15)]^{(2.15)/(0.15)}}} = 7.29 \times 10^{-4}\ m^2 = 7.29\ cm^2$$

Using this calculated throat area and the expansion ratio, the exit area is simply

$$A_2 = \epsilon * A_t = 3.26 * 7.29 \times 10^{-4} = 2.38 \times 10^{-3}\ m^2 = 23.8\ cm^2 \tag{3.7}$$

From the parameters calculated thus far, we can calculate some useful performance metrics such as I_{sp} and thrust coefficient C_F:

$$(I_{sp})_{opt} = F_t/(\dot{m} * g_0) = c/g_0 = 2162.3/9.81 = 220.42\ sec \tag{3.8}$$

where g_0 is the acceleration due to gravity at Earth's surface. C_F is

$$(C_F)_{opt} = \frac{F_t}{p_1 A_t} = \frac{1500}{1.5 \times 10^6 * 7.29 \times 10^4} = 1.372 \tag{3.9}$$

Note that under a more rigorous derivation, C_F can be seen to be a key parameter for analysis and varies depending on γ, the nozzle expansion ratio ϵ, and the pressure ratio p_1/p_2. Normally, C_F is experimentally determined by measuring chamber pressure, throat diameter, and thrust. The optimal C_F and therefore F_t occur when $p_2 = p_3$.

Finally, the physical dimensions of the nozzle can be determined using simple trigonometry via a standard convergence half-angle α of 45° and a standard divergence half-angle β of 15°. The characteristic chamber length L^*, a parameter used for characterizing the necessary chamber volume for adequate mixing and combustion of the propellants, must be more carefully considered. Ideally, L^* is purely a function of the chemistry of the propellant combination and is often based upon previous successful engine designs [3]. However, due to the dynamical and complex nature of nitrous oxide, such as exothermic decomposition after vaporization in the injector and a high density sensitivity to temperature, a more sophisticated model is needed to calculate L^*. Palacz proposes an explicit equation for finding the ideal L^* for a nitrous oxide system, and empirically determined an ideal range for an NO_x/ethanol system of L^* values from 125.6 cm to 167.8 cm [1]. This range is confirmed by Sutton and Biblarz, as L^* values of between 1.0 m and 1.5 m are expected with ethanol systems. A low-range L^* value of 1.25 m was chosen as a smaller form factor is desired over perfect combustion efficiency. L^* is mathematically defined as

$$L^* = \frac{V_c}{A_t} = \frac{\pi r_c^2 Lc}{A_t} \implies L_c = \frac{A_t L^*}{\pi r_c^2} \tag{3.10}$$

where L_c is the length of the chamber and r_c is the radius of the chamber. It is apparent that the desired form factor can be obtained by adjusting either the radius or the length of the chamber. Due to o-ring

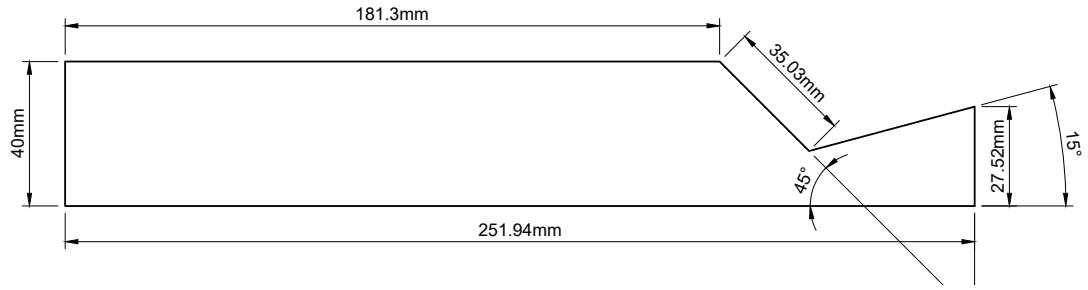

Figure 5: Aphlex 1B drawing with a conical nozzle and given dimensions.

options and standard sizing of metal for the chamber tube, a chamber radius r_c of 3.0 inches was chosen. The only constraint on the chamber radius is the contraction ratio, defined as A_1/A_t (the ratio of chamber area to throat area), which must achieve a value of 4.0 or more [3]. A trivial area calculation can be performed to confirm that this constraint is satisfied: $CR = \pi r_c^2/A_t = 4.56 \times 10^{-3}\ m^2/7.29 \times 10^{-4}\ m^2 = 6.256 > 4.0$. The chamber length is therefore

$$L_c = \frac{A_t L^*}{\pi r_c^2} = \frac{(7.29 \times 10^{-4}\ m^2)(1.25\ m)}{4.56 \times 10^{-3}\ m^2} = 0.19982\ m = 19.982\ cm$$

Calculated Performance Parameters		
Name	Value	Unit
$\dot{m}$, Total mass flow rate	0.694	kg/s
$\dot{m}_f$, Fuel mass flow rate	0.555	kg/s
$\dot{m}_o$, Oxidizer mass flow rate	0.139	kg/s
v_2, Exhaust velocity	2162.3	m/s
$(I_{sp})_{opt}$, Specific impulse (optimal)	220.42	s
$(C_F)_{opt}$, Thrust coefficient (optimal)	1.372	N/A

Table 2: Summary of engine performance parameters.

Calculated Dimensional Parameters		
Name	Value	Unit
α, Convergence half-angle	45	deg
β, Divergence half-angle	15	deg
A_t, Throat area	7.29×10^{-4}	m^2
A_2, Exit area	2.38×10^{-3}	m^2
A_c, Chamber cross-sectional area	4.56×10^{-3}	m^2
R_t, Throat radius	15.23	mm
R_2, Exit radius	27.52	mm
R_c, Chamber radius	38.1	mm
L_c, Chamber length	19.98	mm
ϵ, Expansion ratio	3.26	N/A
CR, Contraction ratio	6.9	N/A

Table 3: Summary of physical nozzle dimensions.

Table 2 shows the calculated engine parameters and Table 3 shows the calculated physical nozzle dimensions. Using the data from Table 3, a basic conical nozzle can be realized.

Figure 5 shows the basic conical nozzle for Aphlex 1B created using the given dimensions. Although a conical nozzle may exhibit an advantage in its ease of manufacturing, it is sub-optimal for performance since 1) the exhaust is not exiting the nozzle completely parallel to the nozzle axis, which results in lateral losses of energy, 2) the sharp convex corner at the throat generates shocks which are not adequately dissipated by a conical nozzle, and 3) the small divergence half-angle ensures a long diverging section, which increases engine mass. To address these issues, most modern nozzles are so-called "bell" nozzles, whose diverging section includes a straightening section to address the first issue and inherently addresses

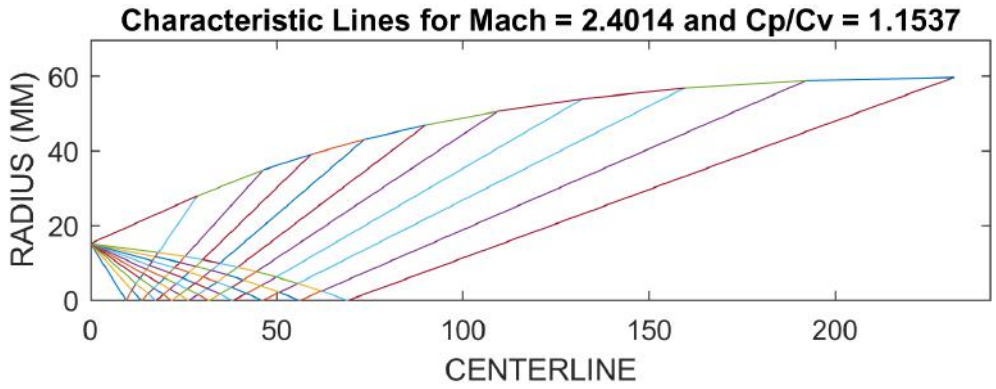

Figure 6: MATLAB visualization for MOC. Shown are the characteristic lines and the generated nozzle contour.

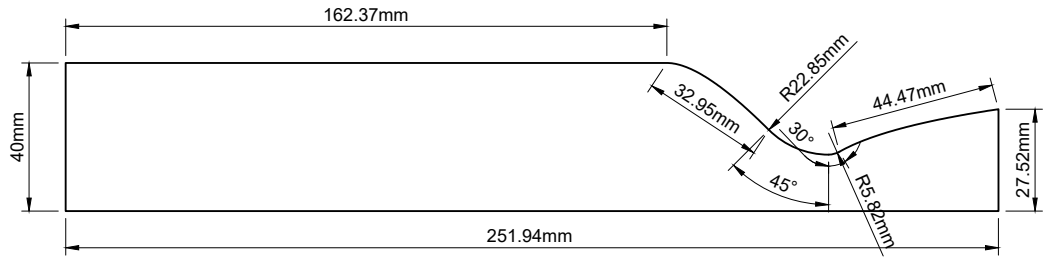

Figure 7: Aphlex 1B drawing with a MOC nozzle and given dimensions.

the third issue by having a more rapidly expanding cross-section as compared to conical nozzles. To neutralize the Prandtl-Meyer expansion fans generated at the sharp corner of the throat, a numerical technique called the Method of Characteristics (MOC) is used to generate the nozzle contour.

In brief, MOC propagates characteristic lines emanating from the throat, and by using equations to model characteristic interactions and reflections, it is able to generate a nozzle contour to precisely neutralize (reflect in a manner parallel to the nozzle axis) these expansion fans. A MATLAB script was written to execute and create the MOC nozzle, which can be found on our Project Caelus propulsion GitHub repository at `https://github.com/ProjectCaelus/propulsion/blob/master/nozzle-calculations/moc_nozzle.m`. Its output is shown in Figure 6. The Cartesian points representing the generated wall contour were exported as a CSV file, which was then imported into our computer-aided design (CAD) program, Fusion 360, where a best-fit nth-order spline was used to finalize the diverging contour. Although the shape of the diverging section can be optimized significantly, the precise shape of the nozzle converging section has not been found to heavily impact engine performance and is therefore smoothed under the guidelines of Dr. GVR Rao's parabolic approximation method [3][2].

3.2 Injector Design

The injector serves two main purposes in a liquid rocket engine: the adequate mixing (atomization) of the incoming propellant streams to ensure maximum combustion efficiency and the prevention or minimization of combustion instabilities. Some injectors additionally implement film cooling to aid in reducing the thermal load of the chamber and nozzle walls, however, our system relies solely on the heat capacity of the chamber walls and a thin ablative layer to maintain wall integrity. This is done since it would save propellant mass that would otherwise be wasted for film cooling and due to the relatively short burn time of our system.

3.2.1 Selection of Element Type

There are many types of injector elements, each with unique advantages and disadvantages. The injector types considered were the triplet (fuel-centered) unlike impinging injector and the like-on-like doublet impinging injector, due to 1) our limited manufacturing capabilities 2) a fairly unbalanced O/F ratio

3) both types exhibiting good mixing and atomization properties and 4) the abundance of historical experience and data with both injector types. Both the coaxial swirl and pintle types were deemed either too complex to manufacture or too difficult to characterize due to a limited amount of available documentation. NASA's SP-8089 conference document on liquid engine injector design suggests that the best way to characterize both the individual orifice geometries and the overall injector geometry for unlike impinging injectors is through diameter ratios. Vigorous cold flow and other empirically testing methods at the time were used and have found correlations between the driving orifice diameter ratio with the optimum mixing efficiency. The correlation found was

$$\left(\frac{d_c}{d_{ou}}\right)^2 = M\left[\frac{\rho_{ou}}{\rho_c}\left(\frac{\dot{m}_c}{\dot{m}_{ou}}\right)^2\right]^{0.7} \tag{3.11}$$

where d_c is the diameter of center orifice, d_{ou} is the diameter of an outside individual orifice, M is an experimentally-determined mixing factor coefficient, ρ represents liquid density, and $\dot{c}$ and $\dot{m}_{ou}$ are the center mass flow rate and outside mass flow rate respectively. It is cited that for a 2-on-1 element type, M has a value of 1.6. Using Equation 3.11, we find that our controlling diameter ratio is

$$\frac{d_c}{d_{ou}} = \sqrt{M\left[\frac{\rho_{ou}}{\rho_c}\left(\frac{\dot{m}_c}{\dot{m}_{ou}}\right)^2\right]^{0.7}} = \sqrt{1.6\left[\frac{772.25\ kg/m^3}{789\ kg/m^3}\left(\frac{0.1389\ kg/s}{0.5556\ kg/s}\right)^2\right]^{0.7}} = 0.4757$$

Since this diameter ratio is not reasonably near 1.22 (as suggested by NASA SP-8089), we can assume this correlation would not be accurate and that there will be potentially drastic losses in mixing efficiency. Thus, this suggests that a like-on-like system is required.

3.2.2 Main Injector Parameterization

Since like-on-like elements will have a 1 to 1 diameter and momentum ratio, we can begin determining the pressure drop and mass flow rate through each individual orifice. Rocket Propulsion Elements (RPE) provides and equation for the volumetric flow rate Q (and therefore $\dot{m}$ since ρ is constant) as shown below:

$$\dot{m} = Q\rho = C_d A\sqrt{2\rho\Delta p} \implies \Delta p = \left[\left(\frac{\dot{m}}{C_d A}\right)^2\right]/2\rho \tag{3.12}$$

where C_d is a dimensionless discharge coefficient that is experimentally determined and a function of the orifice geometry, A is the area of the orifice, and Δp is the pressure drop across the orifice. Flow velocity is similar:

$$v = Q/A = C_d\sqrt{2\Delta p/\rho} \tag{3.13}$$

Since C_d is a measured parameter, initial design calculations must assume a value. RPE suggests a C_d value of around 0.88 for a 1 mm diameter orifice in a short tube with a rounded entrance (assuming an orifice length to diameter ratio of L/D $>$ 3.0), and 0.9 for a similar configuration with a 1.57 mm diameter. Accordingly, a C_d value of 0.9 was chosen for the oxidizer and a C_d value of 0.88 was chosen for the fuel. For the orifice sizing, NASA SP-8089 found that smaller orifice sizes attributed to better mixing in all scenarios, although only to a certain extent (orifice diameters $<$0.03 inches saw insignificant improvements in mixing). Due to limited manufacturing capabilities, a minimum hole size of 1 mm was chosen. Using this information, a design parameter of an overall injector pressure drop that is 25% of chamber pressure, and Equation 3.12, the mass flow rate across a single oxidizer and fuel orifice are

$$\dot{m}_o = 0.9 * (\pi * ((1.58\ mm/2) \times 10^{-3})^2)\sqrt{2(772.25 kg/m^3)(1.5 \times 10^6\ Pa * 0.25)} = 0.0425\ kg/s$$

$$\dot{m}_f = 0.88 * (\pi * ((1.00\ mm/2) \times 10^{-3})^2)\sqrt{2(789 kg/m^3)(1.5 \times 10^6\ Pa * 0.25)} = 0.0168\ kg/s$$

The same pressure drops can be used for each orifice due to Bernoulli's principle and the law of conservation of energy, similar to how voltage stays constant across a parallel circuit. The corresponding injection velocities (Equation 3.13) are

$$v_o = 0.9\sqrt{(2(1.5 \times 10^6\ Pa)(0.25))/(772.25\ kg/m^3)} = 28.048\ m/s$$

$$v_f = 0.88\sqrt{(2(1.5 \times 10^6\ Pa)(0.25))/(789\ kg/m^3)} = 27.132\ m/s$$

Dividing the mass flow rate by the individual orifice mass flow rates gives the total orifice count for each propellant, denoted as n_o and n_f:

$$n_o = \dot{m}_o/\dot{m}_{oi} = (0.4865\ kg/s)/(0.0425\ kg/s) = 11.447$$

$$n_f = \dot{m}_f/\dot{m}_{fi} = (0.139\ kg/s)/(0.0168\ kg/s) = 8.27$$

Since both an integer and even amount of holes are obviously required for a like-on-like impinging injector, Equation 3.12 is rearranged to compute the necessary diameter given the desired number of orifices, given a reasonable range of orifice count provided by the previous calculation:

$$d = 2\sqrt{\frac{\dot{m}}{C_d n \pi \sqrt{2\rho\Delta p}}} \tag{3.14}$$

Solving Equation 3.14 for both oxidizer and fuel streams yields

$$d_o = 2\sqrt{\frac{0.555\ kg/s}{(0.9)(16)\pi\sqrt{2(772.25\ kg/m^3)(1.5\times10^6\ Pa)(0.25)}}} = 0.001428\ m = 1.43\ mm$$

$$d_f = 2\sqrt{\frac{0.139\ kg/s}{(0.88)(8)\pi\sqrt{2(789\ kg/m^3)(1.5\times10^6\ Pa)(0.25)}}} = 0.001017\ m = 1.02\ mm$$

Thus, to achieve 16 oxidizer orifices and 8 fuel orifices, an oxidizer orifice diameter of 1.43 mm and fuel orifice diameter of 1.02 mm are needed.

The remaining injector parameters were chosen due to a literature review, rather than explicit calculations. The angle of impingement, also known as the cant angle λ, is defined as the angle between two propellant jets. It was chosen to be 60 degrees since it is the most common impingement angle, prevents significant backsplash of propellants onto the injector face (which would produce high heat fluxes with unlike elements), and produces the best atomization characteristics despite requiring a larger L^*.

NASA SP-8089 further suggests that the free-stream jet length (impingement length), defined as the distance from an element face to the point of impingement, should be somewhere in the range of five to seven times the orifice diameter. In other words, 5 < L/D ratio < 7. An L/D ratio of 6 was chosen, and the free-stream get length is therefore $(L_{jet})_o = 6 * 1.43\ mm = 8.57\ mm$ and $(L_{jet})_f = 6 * 1.02\ mm = 6.10\ mm$. The point of impingement (distance of impingement orthogonally measured from the injector face) is therefore $(L_{POI})_o = 8.57\ cos(30) = 7.42\ mm$ and $(L_{POI})_f = 6.10\ cos(30) = 5.28\ mm$ since the λ half-angle is 30 degrees.

The thickness of the injector plate is driven by the L/D ratio of the largest orifice (not the jet), which was suggested to be around 10 to ensure smooth and developed flow, assuming the C_d that was used in previous calculations [3]. Simply, $L_{inj} = 10(d_{max})\ cos(\lambda/2)$, since the cosine of the cant half-angle is the coaxial component (thickness). However, a coefficient value of 7 was chosen instead of 10 in the interest of a thinner injector plate. Evaluating gives $L_{inj} = (7)(1.42\ mm)\ cos(30) = 8.608\ mm$. Finally, finding the distance between each orifice within an element pair involves two separate calculations: one for the distance on the side of the injector face (denoted as "combustor-side") and one for the distance on its reverse side (denoted as "manifold-side"). First, the combustor-side distance is $d_{com} = (2)(L_{jet})\ sin(30)$, and therefore, $(d_{com})_o = (2)(8.57\ mm)\ sin(30) = 8.57\ mm$ and $(d_{com})_f = (2)(6.10\ mm)\ sin(30) = 6.10\ mm$. The manifold-side distance is a case of similar triangles with corresponding combustor-side distances: $(d_{man})_o = [(d_{com})_o/(L_{POI})_o](L_{inj} + (L_{POI})_o) = [8.57\ mm/7.42\ mm](8.61\ mm + 7.42\ mm) = 18.512\ mm$. Similarly, by substituting for fuel parameters: $(d_{man})_f = [6.10\ mm/5.28\ mm](8.61\ mm + 5.28\ mm) = 16.045\ mm$. The final injector parameters are summarized in the table below.

3.2.3 Injector Configuration and Assembly Design

The physical configuration of the injector (element pattern) was chosen largely off common practices and previous injector designs. A standard two-ring pattern was implemented, with the outer ring consisting of the four fuel elements and the inner ring consisting of the eight oxidizer elements. The fuel elements were chosen to reside in the outer ring as to reduce the thermal load on the chamber walls, since it would create a fuel-rich region within the combustion volume. No baffles or other dampening devices were utilized since the chamber is of a small enough volume and the burn time is of short enough duration to neglect most instabilities.

Injector Parameters		
Name	Oxidizer (N_2O)	Fuel (C_2H_5OH)
Injector element type	Doublet like-on-like impingement	
ρ, Density at 298 K	772.25 kg/m^3	789 kg/m^3
$\dot{m}$, Mass flow rate	0.5552 kg/s	0.1388 kg/s
C_d, Discharge coefficient	0.90	0.88
n, Number of orifices	16	8
d, Orifice diameter	1.43 mm	1.02 mm
A, Individual orifice area	1.606×10^{-6} m^2	8.171×10^{-7} m^2
Mass flow rate per orifice	0.0347 kg/s	0.01735 kg/s
λ, Angle of impingement	60°	60°
L_{jet}, Free-stream jet length	8.57 mm	6.10 mm
L_{POI}, Point of impingement	7.42 mm	5.28 mm
Length of orifice	10.00 mm	7.11 mm
d_{com}, Distance between orifices (combustor)	8.57 mm	6.10 mm
d_{man}, Distance between orifices (manifold)	18.51 mm	16.05 mm
L_{inj}, Injector plate thickness	8.608 mm	

Table 4: Summary of injector parameters.

For the injector assembly, two designs were considered: Design A and Design B. Design A features two external common bolts that fasten all injector components together (including the chamber wall), making the assembly modular and consisting of smaller parts. Design B requires more material and has a larger vertical profile than Design A, but is also more streamlined, less complex, contains fewer parts, and requires less machining. Design B was heavily inspired from Michigan Aeronautical Science Association (MASA)'s previous injector designs and is therefore also more proven.

For the injector assembly, two designs were considered: Design A and Design B. Design A features two external common bolts that thread through the bottom of the injector plate and radially on the outer rim of the manifold plate, allowing for the entire injector assembly to slide into the chamber tube and be fastened to the chamber wall. Design B includes bolts that thread through the entire injector assembly and into the chamber flange, allowing the injector to sit on top of the chamber. Design B also requires fewer parts, precision, cuts and is more space efficient. Design A was heavily inspired from Michigan Aeronautical Science Association (MASA)'s previous injector design and is therefore more proven.

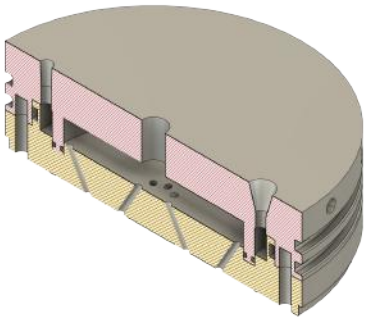

Figure 8: Isometric view of Design A.

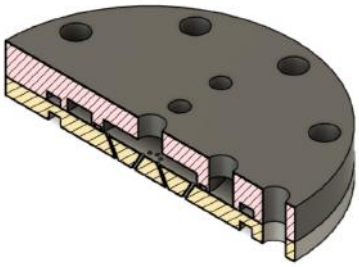

Figure 9: Isometric view of Design B.

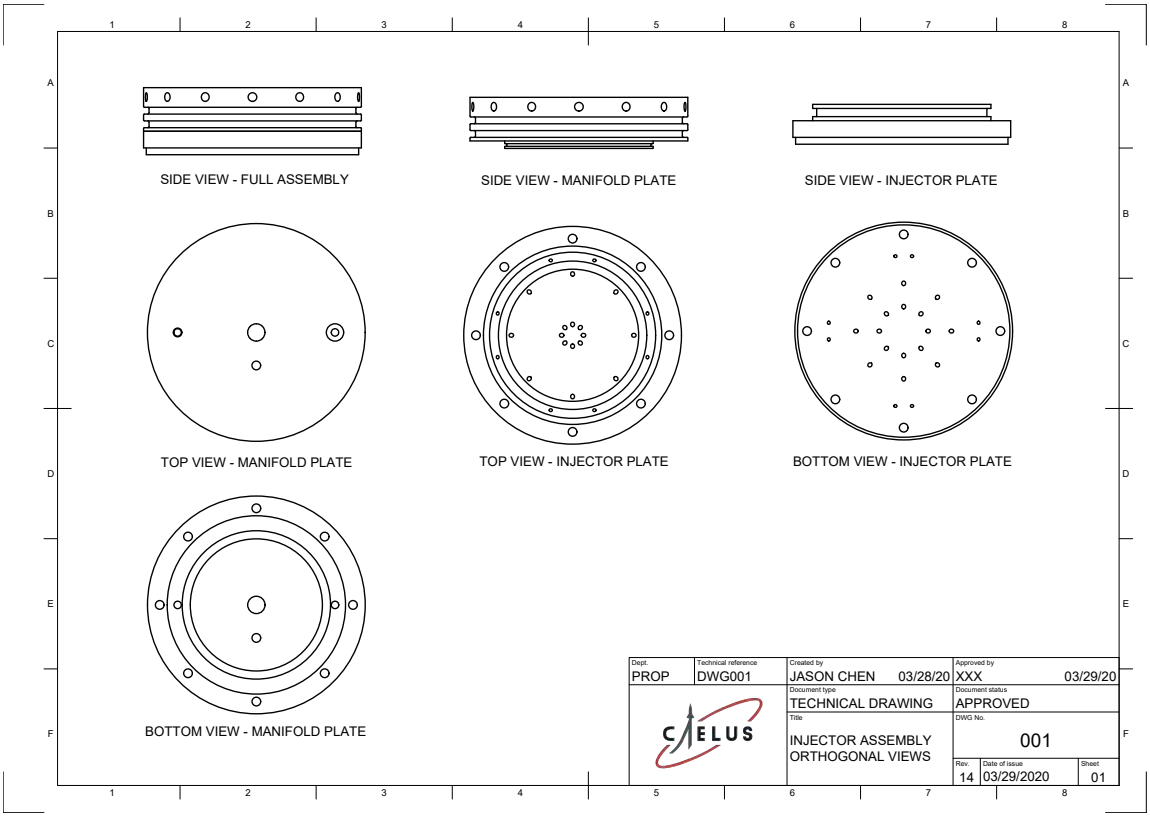

Figure 12: Injector assembly technical drawing orthogonal views.

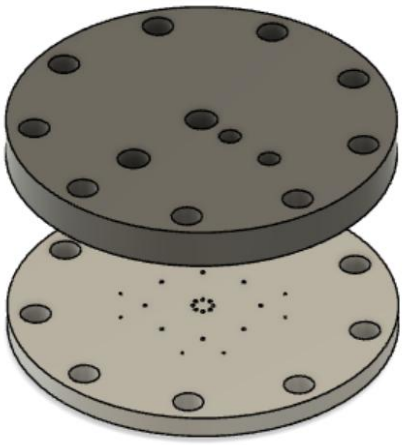

Figure 10: Top exploded view of Design B.

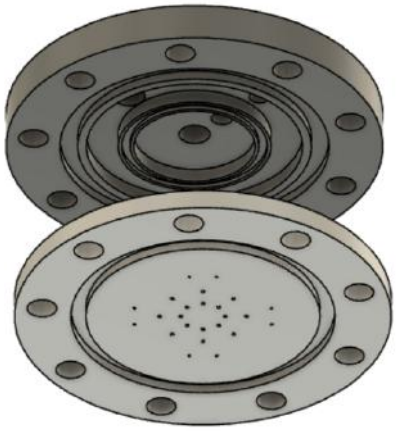

Figure 11: Bottom exploded view of Design B.

Both designs share a design for the component responsible for the separation of the fuel and oxidizer manifolds. Though Design A is more compact and already tested, Design B was ultimately chosen since it requires less manufacturing turn-around, contains fewer bolts and cuts, and has more room for manufacturing flexibility.

Orthogonal and cross-sectional views of Design B (which will henceforth be referred to as simply the "injector assembly") can be seen in Figures 12 and 13. A detailed breakdown of the design is shown in Figure 14 and will be elaborated upon here: the injector assembly comprises of two parts. The manifold plate (1) primarily houses the connection between the main propellant lines and the injector plate. The entirety of the assembly rests on top of the chamber, with the bottom face of the manifold plate housing an o-ring that forms a seal between the combustion chamber and ambient pressure (OR-2

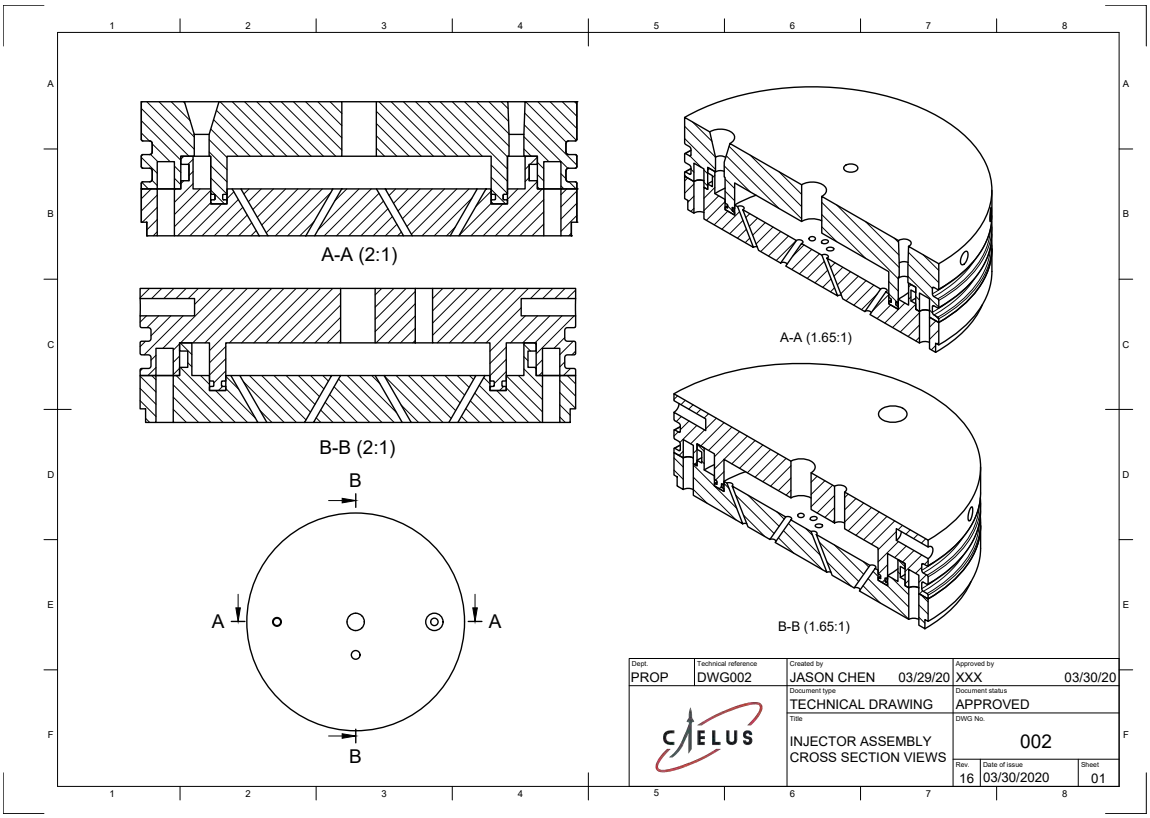

Figure 13: Injector assembly technical drawing cross section views.

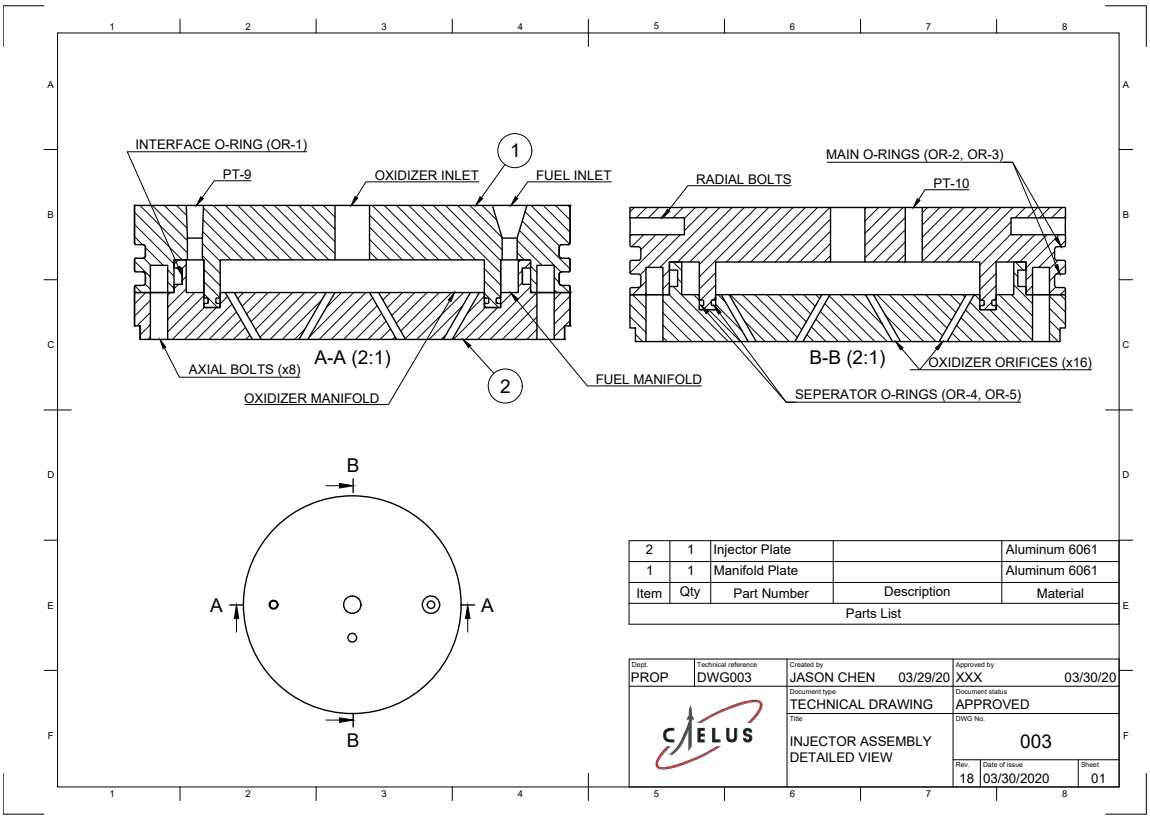

Figure 14: Injector assembly technical drawing detailed description.

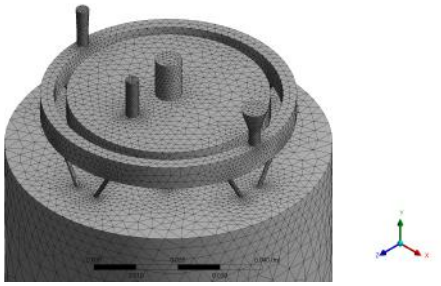

Figure 15: The generated mesh in ANSYS Mesher with ≈197,000 tetrahedron elements.

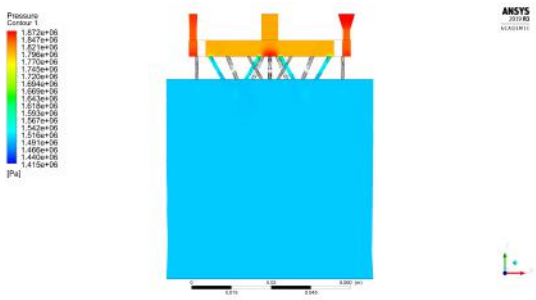

Figure 16: Pressure cross-section contour of the injector assembly and fluid domain.

and OR-3). 9 bolts fasten the injector assembly to the chamber flange and also provide the compression necessary for OR-2 and OR-3 to effectively seal. The main oxidizer inlet is located in the center of the manifold plate and allows the oxidizer to transition into the oxidizer manifold (seen as the central scaffolding). The fuel inlet serves a similar purpose. Both inlets have an entrance diameter of 1/4". The fuel and oxidizer manifolds are divided by a separation ring and are sealed by a separator o-ring (OR-4 and OR-5). PT-9 and PT-10, as the name suggests, are 1/8" ports that allow pressure transducers to access to both manifolds. The injector plate (2) houses the propellant orifices and is in direct contact with the combustion chamber. It was designed deliberately to be as simple as possible so that if the relative difficulty in machining the angled orifices causes a manufacturing error, only the plate itself would need to be discarded and re-machined. Although direct contact with the combustion gases may cause significant heating, the high mass flux of propellant in the propellant manifolds effectively cools the injector plate. An interface o-ring (OR-1) seals the connection between the fuel manifold and the ambient pressure. The chamber diameter and injector diameter were deliberately chosen to allow room for an ablative inside the chamber. The next step in the design of the injector assembly was to verify its flow characteristics, such as flow rates, pressures at certain points, and injection velocities. More accurate estimations for such characteristics would allow for comparisons between expected values and those measured during cold flow tests, and therefore test the integrity of our models. Since the use of explicit fluid flow equations to predict flow characteristics heavily impacted by complex geometries is impractical, a numerical approach through computational fluid dynamics (CFD) was used.

The CFD software used was ANSYS Fluent, which includes a streamlined workflow by providing an integrated geometry editor (SpaceClaim), mesher (ANSYS Mesher), solver (Fluent), and post-processor (CFD-Post). This allowed for a quick verification cycle and even parameterized CFD runs. The injector geometry and fluid domain were created in Fusion 360 and imported into SpaceClaim, where parts and boundaries were labeled for the mesher. The mesh was tetrahedron-based and was discretized to around 197,000 elements. In Fluent, the injector material was set to aluminium and the fluid properties were set to that of ethanol and nitrous oxide at room temperature densities. For the simulation environment, NASA SP-8089 (pp. 35) recommends a pressure drop across the injector between around 15% and 25% of the designated chamber pressure to ensure a steady chamber pressure and prevent feed-coupled instabilities. A liberal Δp of 25% (of P_c) was chosen for this simulation run, i.e. an injector inlet pressure of 1.875×10^6 Pa and outlet pressure (P_c) of 1.50×10^6 Pa was chosen. A more detailed reasoning and explanation for system Δp's is provided in a later section. A steady-state, pressure-based, k-epsilon viscosity model was used for the solver and ran for 1000 iterations. The results were exported into CFD-Post, where volume and cross-section renderings could be made to analyze the results. Report and data files were also generated. Although other many flow characteristics such as turbulence kinetic energy, temperature, and Reynolds Number could be extracted from the results, static pressure and velocity were the most important parameters and are shown in the post-processing rendering.

Figure 16 and its corresponding output files show that the expected Δp from the propellant piping to the manifold is around 75 kPA (around 20% of the total Δp), while majority of the Δp takes place through the orifices, which is expected. It is also notable that the fuel manifold exhibits a significantly shallower Δp than the oxidizer manifold. This is also expected since the fuel manifold has a significantly smaller volume than the oxidizer manifold. Figure 16 displays a cross section that only shows the impingement of the oxidizer elements. Since the pressure profile for the fuel elements is nearly identical but on a different axis, its contour is not shown here.

Figures 17 and 18 show streamlines (contoured to velocity) of the flow through the injector, with

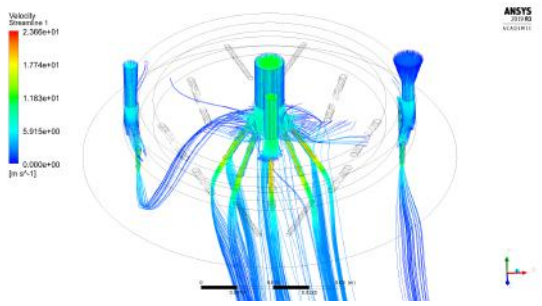

Figure 17: Contoured velocity streamlines (≈2500 streamlines). Note the difference in color between the fuel inlet and PT-9, indicating a reduction in pressure.

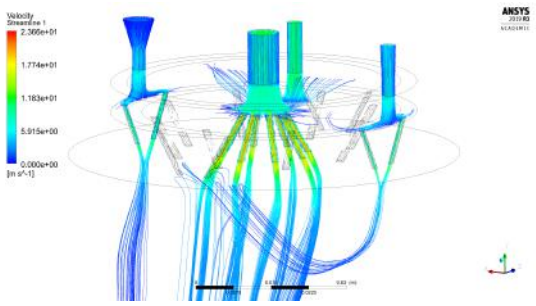

Figure 18: Another view of the contoured velocity streamlines. Note the post-impingement mixing of the outer fuel elements with the inner oxidizer elements.

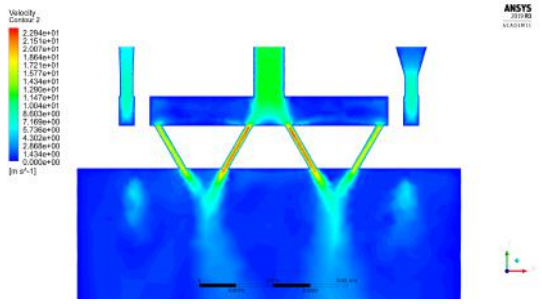

Figure 19: Velocity cross-section contour of the propellant inlets and the oxidizer orifices.

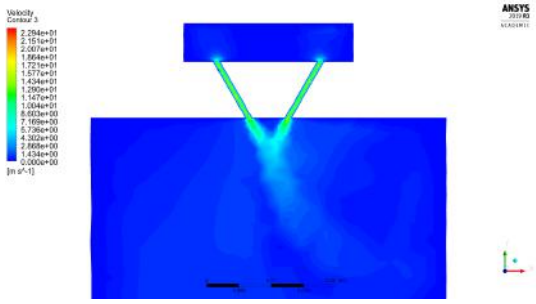

Figure 20: Velocity cross-section contour of fuel orifices. Note the smaller impingement distance.

a wireframe of the injector geometry superimposed. Some streamlines were removed in the interest of visibility and to reduce clutter. Figures 19 and 20 show two velocity contours, one of the oxidizer orifices and one of the fuel orifices. Note how the velocity is greatly increased for the oxidizer orifices near the oxidizer inlet in Figure 19. This is to an advantage in terms of mixing efficiency since it would result in a momentum ratio skewed towards towards the chamber walls, which is where the fuel elements reside, thereby mixing the atomized oxidizer droplets with fuel droplets almost immediately. The velocity traces from fuel impingement can also be seen immediately to the left and right of the oxidizer jets. In Figure 20, the velocity contour for a single fuel element is shown. Both figures indicate that an injection velocity of around 15 m/s can be expected.

3.3 Material Selection, Manufacturing, Load and Thermal Analysis

The final step in the design of the injector, thrust chamber, and nozzle is the selection of materials necessary to fabricate these devices, its means of manufacturing, and how these methods are justified through load and thermal analyses.

3.3.1 Material Selection

Three metals were considered as the primary material for the engine system: aluminium, mild steel, and stainless steel. Mild steel could not be used in areas of combustion or areas in contact with nitrous due to its tendency to react with oxidizers. Stainless steel is more expensive, more difficult to machine, and has a lower specific heat capacity and strength-to-weight ratio than aluminium. For these reasons, aluminium (more specifically, 6061 Aluminium) was chosen as the primary material for the injector assembly, the outermost (structural) wall of the combustion chamber, and the nozzle extension. However, one implication of using aluminium is its incompatibility with threads due to its soft nature. Therefore, as seen in Figure 9, female NPT thread ports will need to be welded onto the top face of the manifold to connect the upstream propellant lines to the injector, and threaded inserts will need to be used to accommodate the radial bolt holes that fasten the combustion chamber wall to the injector assembly.

As mentioned in previous sections, the combustion chamber will rely on an ablative layer, held in place by an outer aluminium structural wall, to dissipate heat generated during combustion. There are many

candidates for this ablative material, however, under the recommendation of MASA and in the interest of costs and simplicity, a phenolic resin ablative, which is a mix of epoxy and wood/fibrous products, became a prime candidate. PVC has also been shown to be an effective and cheap ablative. However, at this time, the material of the chamber ablative has not been finalized. Interestingly, Copenhagen Suborbitals, an extremely successful amateur rocketry organization based in Denmark, has published their findings in mixing tetraethoxysilane (TEOS) with their ethanol solution as an alternative to fixed ablatives. During combustion, TOES decomposes and leaves a thin layer of silicone dioxide (SiO_2) within the chamber walls, acting as a make-shift ablative. All options will be finalized at a later date.

The converging nozzle and especially the throat, which is the site of highest heat flux in the nozzle and combustion chamber, will be shaped out of graphite. Graphite is one of the best and cheapest ablative materials for heat dissipation due to its molecular structure, and has even been used on large-scale launch vehicles. The primary disadvantage of graphite is that large stocks of the material become exponentially more expensive; this is why graphite was not used as the chamber ablative. Since it is expected that the throat ablative will erode most rapidly, perhaps only being useful for one or two engine burns, the entire engine assembly has been made modular as to easily remove and replace the throat when needed. The diverging nozzle section has a significant impact on performance through its geometry and experiences the least heat flux. Therefore, this nozzle section will be fabricated using aluminum.

Another selection process involved choosing an o-ring material. Briefly, o-rings are seals that prevent fluid flow between two (usually) metallic plates. They work by absorbing heat and responding to the released pressure by expanding to fill the groove. Through several references, primarily Parker's O-Ring Handbook and recommendations from collegiate rocketry teams, it was found that the material fluorocarbon (FKM) is well-suited for the injector assembly based on its relatively high heat and pressure tolerance and compatibility with ethanol and nitrous oxide. A specific brand of FKM, Viton, was chosen due to its proven compatibility with nitrous oxide, low price, and accessibility. It was also decided to use a face seal gland since these seals are less likely to fail and are less dependent on manufacturing abilities, as opposed to radial seals. Face seal glands are often utilized when a straight groove is drilled into a flat piece of metal. However, since face seal glands are usually only used at lower temperatures, it is recommended to increase the groove width by some amount to allow for proper expansion of the o-ring in the event that it is exposed to combustion gases.

Parker's O-Ring Handbook also provided guidelines for handling and assembling o-rings. It was mentioned that when assembling the o-ring, stretching it more than 20% of its original length and pinching/twisting the o-ring in any way should be avoided. It is also recommended to lubricate Viton o-rings with lubricant to prevent a spiral failure (when the o-ring is twisted). Krytox lubricant in particular was chosen due to its compatibility with nitrous oxide.

Lastly, metric class 10.9 steel bolts were selected for assembly due to their high proof load of 120,000psi and relatively cheap cost.

3.3.2 Manufacturing Capabilities and Methods

Due to our budget and circumstances, we do not have direct access to any machine shops or manufacturing facilities. We expect the bulk of our manufacturing needs to be met by local services. This further reiterates the emphasis on simple and cost-effective designs since more complex designs will take more time to manufacture, thus increasing costs. The only resources we expect to require, however, are a 5-axis CNC mill (for the injector assembly), a lathe (for the combustion chamber and nozzle), and welding materials.

3.3.3 Load and Thermal Analysis

Although thorough load and thermal analyses can be calculated and simulated precisely, in the scope of Aphlex 1B, it is of secondary priority. Preliminary material stress and load simulations were done in ANSYS APDL and Autodesk Fusion 360's built-in simulation protocol. These simulations verified the structural integrity of the injector assembly, but they were not extensive. To remedy this, care was taken to ensure material thicknesses were adequate to withstand stresses, and fasteners are added liberally to ensure a robust assembly. The primary material thickness (such as on the chamber wall and nozzle wall) was 2.0 mm, which is more than adequate considering the tensile strength of aluminium. It can loosely be verified by the wall thickness equation provided by [4]:

$$t_{wall} = \frac{P_c r_c}{2\sigma_c} \tag{3.15}$$

where σ_c is the stress on the chamber walls. As for thermal loads, the short burn time of between 3 and 7 seconds is adequate enough to prevent significant overheating. The use of ablatives further widened the safety margin.

Extraneous Injector Parameters		
Name	Value	Unit
Δp_{inj}, Pressure drop across injector, relative to P_c	25	%
$(v_{inj})_e$, Injection velocity (expected)	15	m/s
t_{wall}, Wall thickness	2.0	mm
Injector assembly material	Aluminium 6061	N/A
Combustion chamber structural wall material	Aluminium 6061	N/A
Ablative material	Not yet determined	N/A
Diverging nozzle material	Aluminium 6061	N/A
Converging nozzle and throat material	Graphite	N/A
O-ring material	FFKM (FF352)	N/A

Table 5: Extraneous injector parameters.

3.4 Igniter Design

The igniter is the device responsible for providing the initial energy to start the reaction between the propellants. Once this initial energy has been provided, the system will be self-sub staining. The igniter was designed to be as simple as possible while providing reliability. For this purpose, a pyrotechnic method of ignition was chosen. A pyrotechnic igniter utilizes a small amount of solid propellant mounted inside chamber which is then ignited from an external source. To mount the igniter, a simple method of a stick clamped to the nozzle was selected. Potassium chlorate, which is a fairly stable compound, was chosen as the solid propellant which will be used in the igniter. This will allow for an extended burn time over store bought alternatives such as Estes motors. To begin the potassium chlorate reaction, a store bought starter will be utilized. This starter will allow for reliability in starting the potassium chlorate reaction. The starter works by running current through a wire which ingnites pyrogen (a compound that burns when heated) and thus begins the overall ignition process.

3.5 Engine assembly

The engine assembly is a modular process with testing along the way that ensures everything is working properly. The first two stages consists of the CNCing of the main pieces coupled with the assembly of the engine. After this, the engine will be used in a hydrostatic test to ensure it is working properly. Once the engine assembly has been verified to be working, the chamber tube, 2 chamber flanges well as the nozzle rod and the nozzle flange will be welded. Once again the system will undergo a hydrostatic test but this time to ensure the welds are complete. After a successful test, the engine will once again be dissembled to prepare it for a full cold flow test. This preparation will include inserting the ablative that will be used in a later hot fire test. This test will not only complete a full cold flow but will ensure the injector works through an injector spray test.

4 Plumbing System Design

The design of the plumbing system, the system responsible for carrying the propellant from the propellant tanks to the engine, is a process that is heavily intertwined with ground operations, software design, safety procedures, and the engine design. Due to the complexity of the design process, this section will be partitioned into two sections: a general system design, such as how pressure drops affect tank requirements, piping sizing, and selecting valve trades, and operational design, such as specific filling, pressurization, and safety procedures.

4.1 General System Design

The first step in designing a liquid rocket engine plumbing system involves finalizing the engine cycle. The engine cycle describes the method in which pressurization can be achieved such that the propellants

flow follow a positive pressure gradient out of the tanks and into the engine. This may include the use of turbopumps (whether this be driven electrically or with a pre-burner), expander cycles (which use a heat exchanger at the combustion chamber and nozzle to further pressurize the propellant lines), combustion tap-offs, inert gases, or a myriad of other methods. Upholding the philosophy of cost-effectiveness and simplicity, the pressurization of the propellant tanks via an inert gas was chosen (also referred to as a pressure-fed cycle). It requires the least amount of parts and is by far the simplest option.

There are two basic options with a pressure-fed cycle: regulated or unregulated. In a regulated design, there is a separate pressure vessel containing the pressurizing gas, which flows through a regulator and into the main propellant tanks. This regulator serves to maintain a constant pressure even as the propellant in the tanks are expended. In a unregulated design, also known as a blowdown design, the pressurant is stored inside the main propellant tank along with the liquid propellant. This has the obvious disadvantage of exhibiting a dynamic and decaying chamber pressure. A blowdown design was nevertheless selected for its simplicity. It should be noted that only the ethanol tank would require a pressurant and blowdown system, since the nitrous tank is self-pressurizing.

The pressurant gas selection was a straightforward tradeoff. Typically, the pressurizing gas is an inert gas (one that does not react with the liquid propellant it is pressurizing), which leaves essentially two options for the designer: helium or nitrogen. Any gases further down the periodic table are deemed too heavy with no significant advantage. Though helium lighter and is often used with liquid oxygen (LOX) systems since nitrogen dissolves in LOX, it is significantly more expensive. For these reasons, nitrogen was chosen as the pressurant.

With the engine cycle and pressurant determined, a general plumbing system design can be realized. A piping and instrumentation diagram (P&ID) is an overarching flow diagram that details the interactions and connections of parts throughout the entire plumbing system. P&IDs are the standard for representing rocket propulsion plumbing systems and therefore, much care was taken in its conception. All parts of the P&ID have been carefully examined and optimized to fit the mission needs.

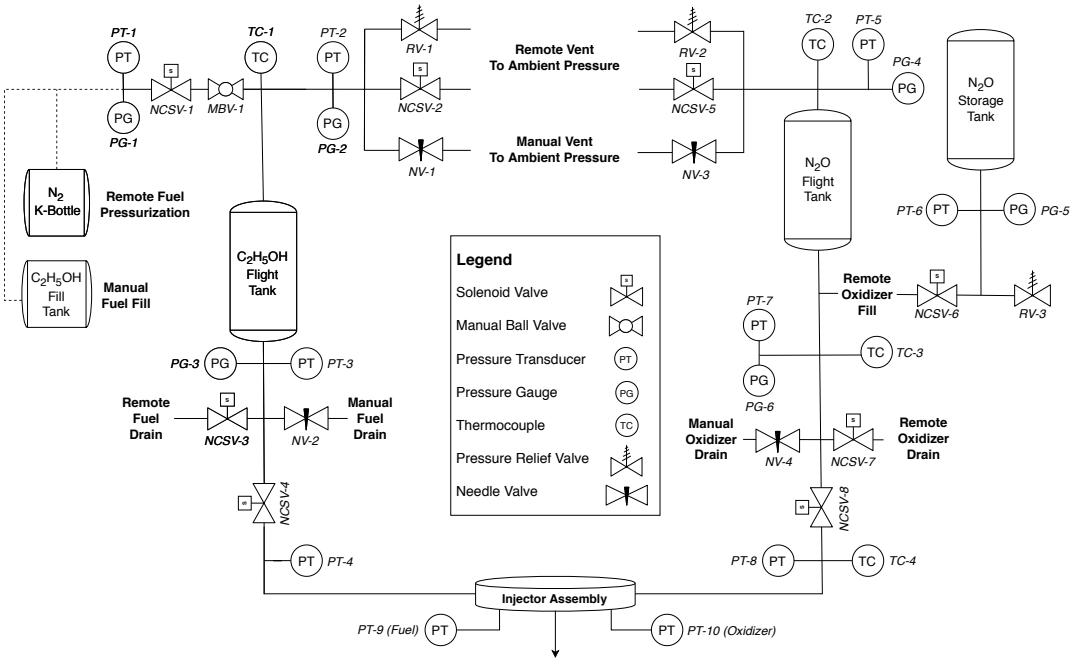

Figure 21: Full system piping and instrumentation diagram (P&ID).

The mechanical and procedural aspects of the P&ID, such as reasoning for fill system procedures and valve types, will be discussed in a later section. Here, attention should be drawn to the general design aspects of the P&ID. First, note the symmetry between both propellant towers. Only the fill and pressurization systems differ. The fill and pressurization tanks (ethanol) directly empty into the flight tank, which indicates the blowdown design. The nitrous flight tank is simply filled by gravity via the nitrous storage tank. During both fill and flight conditions for both towers, a remote and ambient vent of the pressurant is available. Pressure is measured here to monitor tank pressurization and depletion profiles. A thermocouple is also placed here, but is only really necessary on the nitrous tower due to

its density and boil rate sensitivity to temperature. Only one valve lies between the flight tank and the injector: the main propellant valve (MPV). The MPV is responsible for simply opening or closing propellant flow to the engine. The MPV is a solenoid valve since proportional control via a ball valve was deemed unnecessary; there is no intention for engine throttling and concerns for a hard start in startup transients can be addressed with a properly designed ignitor and robust flight software. Instruments are placed on either side of the MPV to measure pressure losses, and therefore its C_v. A pair of remote and manual drain valves was placed before the MPV to divert propellants away from the engine in case of an MPV failure or system over-pressurization that cannot be addressed solely by the vent system. No purge lines were implemented since residual propellants inside the propellant lines are not a significant safety concern (neither propellants are particularly toxic or cryogenic).

With a P&ID drafted, the next step becomes to determine the physical characteristics of the plumbing system, such as tank dimensions, pipe diameters, valve trades, and flow characteristics.

4.2 System Pressure Drop Δp_{sys}

The first and most important step to conceptualizing the physical characteristics of the plumbing system is to determine the required tank volumes and pressures. The tank pressure and pressure profile drives every component downstream of it, which is effectively the entire system. But to achieve this, it is necessary to first determine the pressure drops expected throughout the plumbing system so that a minimum final tank pressure can be set. This is done as to prevent blowback from the combustion chamber near the end of an engine burn and represents the expected final system state. Characterizing the expected pressures at different points within the system is also useful as expected values when comparing to empirical data. This total sum of pressure drops between the propellant tank and combustion chamber, Δp_{sys}, can be decomposed into individual part loses (flow barriers such as valves), frictional loses through the raw length of the pipe (head loss and other effects), and the injector Δp. Mathematically:

$$\Delta p_{sys} = \Delta p_{inj} + \Delta p_{val} + \Delta p_{ext} \tag{4.1}$$

The previous section has already established that Δp_{inj} obtains a value of 25% P_c, which evaluates to $\Delta p_{inj} = 375\ kPa$. The remaining two terms will be elaborated upon further in the following subsections.

4.2.1 Pipe Length and Extraneous Pressure Losses Δp_{ext} [1]

Modelling compressible viscous flow through a pipe is a nontrivial task. To avoid lengthy theoretical calculations that would otherwise be overshadowed by empirical data anyway, assumptions were made about the fluid flow to simplify the pipe sizing and pressure loss calculations. The two most important of these assumptions are that 1) there are no swirl, entrance, or heat-transfer effects, and 2) the pipe is completely circular. A short derivation for the necessary equations for calculating Δp_{ext} starts simply with the classic case of Bernoulli's Equation:

$$p + \frac{1}{2}\rho V^2 + \rho g_0 z = constant \tag{4.2}$$

It gives insight into the balance between pressure, velocity, and elevation by assuming that the two points in question lie on a streamline, the fluid is incompressible, the flow is steady and inviscid, and there is no friction. Although useful for some applications, it is not adequate for designing robust piping systems which will in actuality encounter such effects.

The addition of a *head loss* term, denoted as h_f, is important in introducing a viscous term in an otherwise inviscid equation. Head loss can simply be thought of as an additional pressure loss in the system due to viscous effects, a sudden expansion/contraction, and/or obstructions to its path such as pipe elbows, bends, valves, etc. To introduce the head loss term into a useful form for solving pipe flow problems, there is the famous *Darcy-Weisbach equation*, which is a proposed correlation valid for duct flow of any cross section and any Reynolds Number:

$$h_f = f\frac{L}{d}\frac{V^2}{2g} \tag{4.3}$$

[1] In the following subsection, some explanatory tools, such as derivations and figures, are heavily inspired from the work of [5]. Any figures extracted from [5] are strictly for the purpose of visualization, explanation, and education. We make no claims and have no intention in claiming ownership or rights to these graphics.

The dimensionless parameter f is the *Darcy friction factor*, which establishes a relationship between roughness and pipe resistance. ϵ is the wall roughness height, which is significant only in turbulent pipe flow. It has been shown that ϵ has orders of magnitude *less of an effect* on laminar pipe flow. An alternative form of the friction factor is

$$\frac{8\tau_w}{\rho V^2} = f = F(Re_d, \frac{\epsilon}{d}) \tag{4.4}$$

where F represents some relationship between the Reynolds Number Re_d and the average pipe roughness to diameter ratio ϵ/d (also known as relative roughness).

Piping Design Parameters		
Name	Value	Unit
Oxidizer	Nitrous oxide (at 298 K)	N/A
Fuel	Ethyl alcohol (95%)	N/A
μ_o, Dynamic viscosity (oxidizer)	0.00147	$kg/m \cdot s$
μ_f, Dynamic viscosity (fuel)	0.001232	$kg/m \cdot s$
ρ_o, Density (oxidizer)	772.25	kg/m^3
ρ_f, Density (fuel)	789	kg/m^3
L, Pipe length	2.0	m
d, Pipe diameter	6.35	mm
$\dot{m}_o$, Oxidizer mass flow rate	0.555	kg/s
$\dot{m}_f$, Fuel mass flow rate	0.139	kg/s
Pipe material	316 stainless steel	N/A
ϵ, Roughness	0.5 to 1.5	μm

Table 6: Design parameters and fluid properties required for pipe calculations.

Table 6 shows the piping parameters necessary for following calculations. For the purposes of demonstration, the calculation involving ethanol will be done first. The pipe length was estimated using a model of the test stand discussed in a later section, but is a very conservative estimate. The pipe diameter is constrained to a value of 6.35 mm (1/4 inch) due to budget constraints on the MPV, which houses a 1/4 inch port. The roughness ϵ is based on the pipe material and was extracted from engineering databases.

The behavior of turbulent and laminar flows are significantly different when considering flow characteristics of a viscous flow through a frictional pipe. Thus, it is important to determine which type of flow is expected. Using values from 6, we quickly realize our flow is most likely turbulent

$$Q = \frac{\dot{m}_f}{\rho} = \frac{0.139\,kg/s}{789\,kg/m^3} = 1.762 \times 10^{-4}\,m^3/s \tag{4.5}$$

$$v = \frac{Q}{\pi R^2} = \frac{(1.762 \times 10^{-4}\,m^3/s)}{\pi[(0.00635\,m)/2]^2} = 5.563\,m/s \tag{4.6}$$

$$\nu = \frac{\mu}{\rho} = \frac{0.001232\,kg/m \cdot s}{789\,kg/m^3} = 1.56 \times 10^{-6}\,m^2/s \tag{4.7}$$

$$Re_d = \frac{vd}{\nu} = \frac{(5.563\,m/s)(0.00635\,m)}{1.56 \times 10^{-6}\,m^2/s} = 22644 \tag{4.8}$$

since $Re_d >> 2300$ (a Reynolds Number above 2300 is the accepted threshold). Though many differences are present between turbulent and laminar flow in the context of fluid flow through a pipe, perhaps the most important is that the head loss and pressure drop in turbulent flows are heavily affected by pipe roughness. In fact, there are different sets of equations applied when solving for turbulent flows, depending on the relative roughness of the pipe it is travelling through. These categories are [5]

$$\frac{\epsilon u^*}{\nu} < 5 = \textit{hydraulically smooth} \text{ walls, no effect of roughness on friction}$$

$$5 \leq \frac{\epsilon u^*}{\nu} \leq 70 = \textit{transitional} \text{ roughness, moderate Reynolds Number effect}$$

$$\frac{\epsilon u^*}{\nu} > 70 = \textit{fully rough} \text{ flow, sublayer broken up and friction independent of } Re$$

For a smooth-walled pipe, the relation between friction factor and Reynolds Number for turbulent pipe flow is

$$\frac{1}{f^{1/2}} = 2.0\,log(Re_d\,f^{1/2}) - 1.8 \tag{4.9}$$

An alternate form of equation 4.9 can be used to explicitly solve for f from Re_d:

$$f = \begin{cases} 0.316Re_d^{-1/4} \\ \left(1.8\,log\frac{Re_d}{6.9}\right)^{-2} \end{cases} \quad \text{when } 4000 < Re_d < 10^5 \tag{4.10}$$

For correlating pipe friction to Reynolds Number, although for a limited range of low turbulent Reynolds Numbers, from Equation 4.10 it was was derived that

$$h_f = \frac{\Delta p}{\rho g} = f\frac{L}{d}\frac{V^2}{2g} \approx 0.316\left(\frac{\mu}{\rho V d}\right)^{1/4}\frac{L}{d}\frac{V^2}{2g} \tag{4.11}$$

or

$$\Delta p \approx 0.158L\rho^{3/4}\mu^{1/4}d^{-5/4}V^{7/4} \tag{4.12}$$

Substituting $Q = \frac{1}{4}\pi d^2 V$ into Equation 4.12 gives

$$\Delta p \approx 0.241L\rho^{3/4}\mu^{1/4}d^{-4.75}Q^{1.75} \tag{4.13}$$

Equation 4.13 is critical to understanding pipe sizing. Analysing Equation 4.13 shows that for a fixed flow rate Q, the turbulent pressure drop decreases with diameter every sharply. Thus, the easiest way to reduce required pumping/upstream pressure is to increase the pipe diameter.

For fully rough flows (independent of Reynolds Number):

$$\frac{1}{f^{1/2}} = -2.0\,log\frac{\epsilon/d}{3.7} \tag{4.14}$$

To model the transitionally rough range, an general interpolation formula was created:

$$\frac{1}{f^{1/2}} = -2.0\,log\left(\frac{\epsilon/d}{3.7} + \frac{2.51}{Re_d\,f^{1/2}}\right) \tag{4.15}$$

Equation 4.15 is the accepted formula for determining turbulent friction. Plotting this relation gives the *Moody chart* for pipe friction (see Figure 22). Equation 4.15 is sometimes cumbersome to evaluate for f if Re_d is known, so an alternate explicit formula was developed and as

$$\frac{1}{f^{1/2}} \approx -1.8\,log\Big[\frac{6.9}{Re_d} + \left(\frac{\epsilon/d}{3.7}\right)^{1.11}\Big] \tag{4.16}$$

and varies less than 2 percent from Equation 4.15 [5].

The head loss and Δp values can now be computed using the Moody Chart (Figure 22) and/or Equation 4.16. Once again recalling parameters given in Table 6 and the short velocity and Reynolds number calculations given below Table 6, these values can directly be inserted into Equation 4.16 to find the friction factor f:

$$\frac{1}{f^{1/2}} \approx -1.8\,log\Big[\frac{6.9}{Re_d} + \left(\frac{\epsilon/d}{3.7}\right)^{1.11}\Big]$$

$$f = \left(-1.8\,log\left[\frac{6.9}{22644} + \left(\frac{(1.5\times10^{-6}\,m)/(6.35\times10^{-3}\,m)}{3.7}\right)^{1.11}\right]\right)^{-2} = 2.540\times10^{-2}$$

Now using Equation 4.11 we can find the head loss h_f:

$$h_f = \frac{\Delta p}{\rho g_0} = f\frac{L}{d}\frac{V^2}{2g_0}$$

$$h_f = (2.540\times10^{-2})\left(\frac{2.0\,m}{6.35\times10^{-3}\,m}\right)\left(\frac{(5.563\,m/s)^2}{2(9.81\,m/s)}\right) = 12.62\,m$$

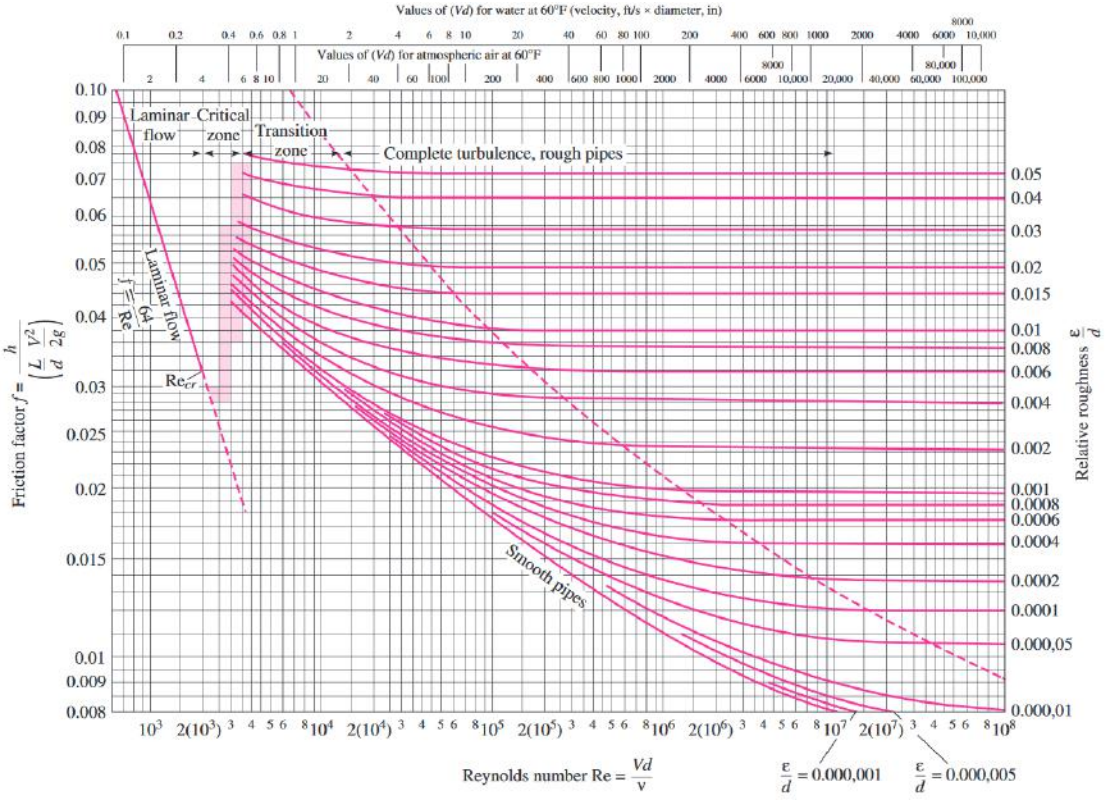

Figure 22: The Moody Chart [5].

The Δp_{ext} is therefore simply

$$\Delta p = h_f \rho g_0 = (12.62\,m)(789\,kg/m^3)(9.81\,m/s^2) = 97669\,Pa \approx 97.7\,kPa$$

This pressure drop of around 100 kPa is reasonable, especially for a 1/4 inch pipe. The flow velocity v of 5.563 m/s is moderately fast, but still reasonable. A literature review showed that it is recommended to maintain a fluid velocity of no more than 6 m/s [Zucrow Laboratories] to avoid significant water hammer effects in case of a valve shutoff, as well as to decrease the Reynolds Number. A fluid velocity of $v = 5.563\,m/s$ just barely satisfies this recommendation, and so care should be taken to not initiate abrupt valve shutoffs if possible.

Figure 23 shows the effect of varying pipe diameters and pipe roughness on the expected pressure drop from head loss. The source code can be found at `https://github.com/ProjectCaelus/propulsion/blob/master/fluid-flow-calculations/pipePressureLossCalc.m`. It is apparent that by the exponential nature of the relationship between diameter and Δp that the best method of reducing Δp is by widening the diameter; a two-fold increase in diameter yields around a four-fold decrease in pressure drop. Although previously it was discussed that pipe roughness has a larger impact on the Δp of turbulent flow than laminar flow, it is clear from Figure 23 that this effect is still relatively small.

This process can be repeated for the nitrous tower. Using a mass flow rate $\dot{m}_o$ of 0.555 kg/s, dynamic viscosity μ_o of $0.00147\,kg/m \cdot s$, Equations 4.16 and 4.11, and updating the fluid velocity, kinematic viscosity, and Reynolds Number from Equations 4.5, 4.6, 4.7, and 4.8, Δp_{ext} is recalculated:

$$Q = \frac{\dot{m}_o}{\rho} = \frac{0.555\,kg/s}{772.25\,kg/m^3} = 7.187 \times 10^{-4}\,m^3/s$$

$$v = \frac{Q}{\pi R^2} = \frac{(7.187 \times 10^{-4}\,m^3/s)}{\pi[(0.00635\,m)/2]^2} = 22.69\,m/s$$

$$\nu = \frac{\mu}{\rho} = \frac{0.00147\,kg/m \cdot s}{772.25\,kg/m^3} = 1.904 \times 10^{-6}\,m^2/s$$

$$Re_d = \frac{vd}{\nu} = \frac{(22.69\,m/s)(0.00635\,m)}{1.904 \times 10^{-6}\,m^2/s} = 75673$$

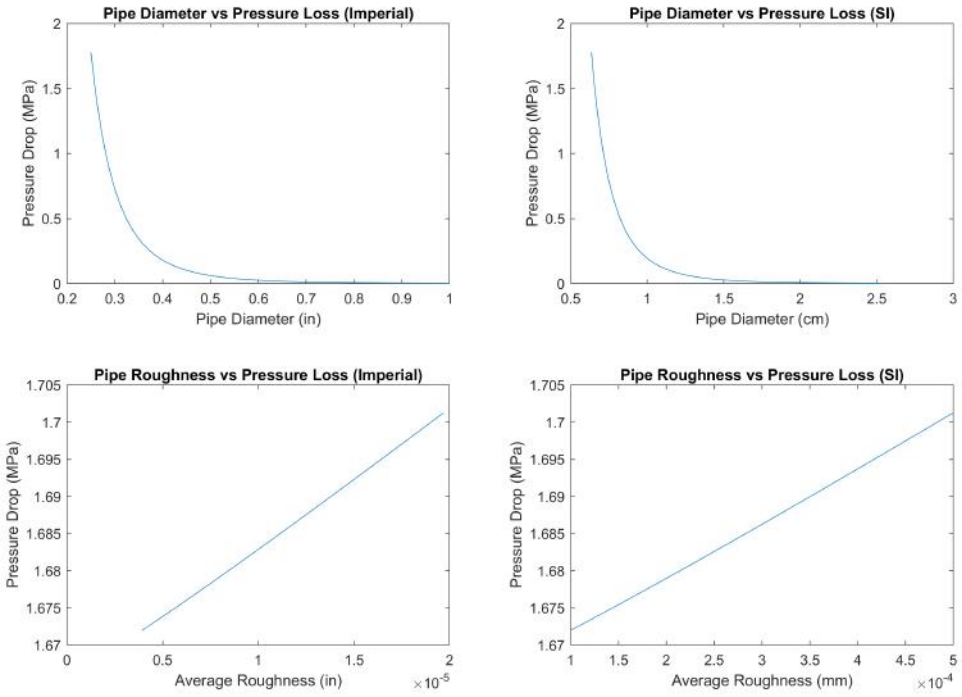

Figure 23: Pressure drops for varying pipe diameters and pipe roughness using flow parameters specified in Table 6. Both imperial and SI units are provided.

$$f = \left(-1.8\, log \left[\frac{6.9}{75673} + \left(\frac{(1.5 \times 10^{-6}\, m)/(6.35 \times 10^{-3}\, m)}{3.7} \right)^{1.11} \right] \right)^{-2} = 1.982 \times 10^{-2}$$

$$h_f = (1.982 \times 10^{-2}) \left(\frac{2.0\, m}{6.35 \times 10^{-3}\, m} \right) \left(\frac{(22.69\, m/s)^2}{2(9.81\, m/s)} \right) = 163.8\, m$$

$$\Delta p = h_f \rho g_0 = (163.8\, m)(772.25\, kg/m^3)(9.81\, m/s^2) = 1240957\, Pa \approx 1.24\, MPa$$

This pressure drop is unacceptable. With a pressure drop purely due to head loss almost as high as the chamber pressure, it is unreasonable to continue design with 1/4 inch piping. Typically, pressure losses due to pipe length are negligible since the higher flow rates and wider pipe diameters reduce the head loss term and flow velocity significantly. However, as mentioned previously, this design is constrained to a pipe diameter of 6.35 mm (1/4 inch) due to the MPV. Thus, since the only solution to reducing head loss is either widening or reducing the length of the pipe, the best course of action is to increase the system pipe diameter to 1/2 inch (12.7 mm) and to use a reducing adapter to accommodate the MPV. Although the reducer will produce head loss and a pressure drop of its own, it is insignificant compared to the 1.24 MPa pressure drop as expected from a universal 1/4 inch pipe system. It was decided to implement a 1/2 inch system for the ethanol tower as well in the interest of consistency.

Using a pipe diameter d of 12.7 mm for both propellants, Δp_{ext} is recalculated. First, for ethanol:

$$v = \frac{Q}{\pi R^2} = \frac{(1.762 \times 10^{-4}\, m^3/s)}{\pi[(0.0127\, m)/2]^2} = 1.391\, m/s$$

$$Re_d = \frac{vd}{\nu} = \frac{(1.391\, m/s)(0.0127\, m)}{1.56 \times 10^{-6}\, m^2/s} = 11324$$

$$f = \left(-1.8\, log \left[\frac{6.9}{11324} + \left(\frac{(1.5 \times 10^{-6}\, m)/(1.27 \times 10^{-2}\, m)}{3.7} \right)^{1.11} \right] \right)^{-2} = 3.000 \times 10^{-2}$$

$$h_f = (3.000 \times 10^{-2}) \left(\frac{2.0\, m}{1.27 \times 10^{-2}\, m} \right) \left(\frac{(1.391\, m/s)^2}{2(9.81\, m/s)} \right) = 0.466\, m$$

$$\Delta p = h_f \rho g_0 = (0.466\,m)(789\,kg/m^3)(9.81\,m/s^2) = 3606.2\,Pa \approx 3.61\,kPa$$

Thus, $\Delta p_{ext} = 3.61\,kPa$ for a 1/2 inch pipe system (ethanol tower), which is more than one order of magnitude less than that of a 1/4 inch pipe system. A fluid velocity $v = 1.391\,m/s$ is also comfortable given the $v < 6\,m/s$ guideline as mentioned before. For nitrous:

$$v = \frac{Q}{\pi R^2} = \frac{(7.187 \times 10^{-4}\,m^3/s)}{\pi[(0.0127\,m)/2]^2} = 5.673\,m/s$$

$$Re_d = \frac{vd}{\nu} = \frac{(5.673\,m/s)(0.0127\,m)}{1.904 \times 10^{-6}\,m^2/s} = 37840$$

$$f = \left(-1.8\,log\left[\frac{6.9}{37840} + \left(\frac{(1.5 \times 10^{-6}\,m)/(1.27 \times 10^{-2}\,m)}{3.7}\right)^{1.11}\right]\right)^{-2} = 2.236 \times 10^{-2}$$

$$h_f = (2.236 \times 10^{-2})\left(\frac{2.0\,m}{1.27 \times 10^{-2}\,m}\right)\left(\frac{(5.673\,m/s)^2}{2(9.81\,m/s)}\right) = 5.776\,m$$

$$\Delta p = h_f \rho g_0 = (5.776\,m)(772.25\,kg/m^3)(9.81\,m/s^2) = 43758\,Pa \approx 43.8\,kPa$$

Piping System Calculated Parameters (Δp_{ext})		
Name	Oxidizer (N_2O)	Fuel (C_2H_5OH)
Q, Volumetric flow rate	$7.187 \times 10^{-4}\ m^3/s$	$1.762 \times 10^{-4}\ m^3/s$
v, Flow velocity	$5.673\ m/s$	$1.391\ m/s$
ν, Kinematic viscosity	$1.90 \times 10^{-6}\ m^2/s$	$1.56 \times 10^{-6}\ m^2/s$
Re_d, Reynolds Number	37840	11324
f, Darcy friction factor	2.236×10^{-2}	3.000×10^{-2}
h_f, Head loss	$5.776\ m$	$0.466\ m$
Δp_{ext}, Pressure drop	$43.8\ kPa$	$3.61\ kPa$
d, Pipe diameter	$12.7\ mm$	
L, Pipe length	$2\ m$	

Table 7: Summary of calculated piping system parameters.

4.2.2 Valve C_v Pressure Drop (Δp_{val})

The second term in determining system pressure drop arises from losses due to geometric obstructions to the propellant flow path. This may include any object, such as valves, pipe elbows, adapters, or other obstructions. To describe the relationship between pressure drop and volumetric flow rate for any object in the flow path, a valve flow coefficient, or C_v is used. C_v is an experimentally-determined coefficient and is defined as

$$C_v = Q\sqrt{\frac{S_G}{\Delta p}} \tag{4.17}$$

where S_G is the specific gravity of the fluid, defined as the ratio of its density to the density of water (ρ_x/ρ_{H2O}). The C_v equation is typically used with imperial units (gal/min and psi), and this convention will be followed here. Revisiting the P&ID (Figure 21) reveals that the only significant obstruction in flow for both propellant towers is the MPV. The specific MPV model (18070NOS from Holley/NOS) was chosen due to its low price and compatibility with nitrous oxide. As mentioned previously, it has a 1/4 inch diameter and will require two reducing adapters for compatibility with the main 1/2 inch propellant lines. Since the MPV is a solenoid, a relatively low C_v value (and therefore, higher pressure drop) is expected. With the assistance of MASA's previous cold flow tests, a C_v value of 0.7 is expected for the MPV. Thus, the Δp for both propellants can be calculated. Rearranging Equation 4.17 to solve for Δp gives

$$\Delta p = \frac{S_G Q^2}{(C_v)^2} \tag{4.18}$$

Calculating for both propellants:

$$\Delta p_o = \frac{S_G Q^2}{(C_v)^2} = \frac{(0.772)(11.392\ gal/min)^2}{(0.7)^2} = 204.47\ psi (\approx 1.410\ MPa)$$

$$\Delta p_f = \frac{S_G Q^2}{(C_v)^2} = \frac{(0.789)(2.793\ gal/min)^2}{(0.7)^2} = 12.56psi (\approx 86.60\ kPa)$$

Though the expected Δp for the nitrous MPV is painfully high, it is unavoidable. An arbitrarily chosen additional 50 kPa pressure drop was added to both Δp estimates to accommodate for additional losses due to pipe bends and adapters. Thus, the final Δp_{val} for each propellant are:

$$(\Delta p_{val})_o = 1.460\ MPa$$

$$(\Delta p_{val})_f = 130.60\ kPa$$

4.2.3 System Pressure Drop (Δp_{sys})

Finally, using Equation 4.1, the system pressure drops for both propellants can be determined:

$$(\Delta p_{sys})_o = \Delta p_{inj} + \Delta p_{val} + \Delta p_{ext} = 375\ kPa + 1.460\ MPa + 43.8\ kPa = 1.879\ MPa \tag{4.19}$$

$$(\Delta p_{sys})_f = \Delta p_{inj} + \Delta p_{val} + \Delta p_{ext} = 375\ kPa + 130.60\ kPa + 3.61\ kPa = 509.2\ kPa \tag{4.20}$$

4.3 Tank Sizing

With the system pressure drop determined, the next step in the design of the plumbing system is to determine the initial tank pressure and tank volume. To find the tank volume requirement, the tank *ullage* must be first determined. The ullage in a propellant tank is simply the percentage of tank volume that is not occupied by the propellant itself, i.e. the space that the pressurant occupies. Though complex models may be developed to more accurately model the expansion of the pressurant as the tank drains, it is commonly excepted that either the ideal gas law ($P_1V_1 = P_2V_2$) or an isentropic expansion model is adequate. It is apparent that due to the ideal gas law, a larger ullage is desirable since it would cause a more stable chamber pressure throughout engine operation to be observed. A literature review was conducted and showed that common practice involved a ullage fraction of around 2/3 (via Copenhagen Suborbitals and MASA). As for the nitrous tank, the process for determining a ullage fraction is nontrivial. Since the vaporization rate, along with many other dynamical aspects of nitrous behavior, is nonlinear and difficult to determine, either sufficiently complex models or reference data is required. A review of many cold-flow and hot-fire tests (especially those from participants in the Intercollegiate Rocket Engineering Competition, or IREC) was conducted, particularly examining the plots of pressure profiles for nitrous oxide. It was found, along with advisories from MASA, that the nitrous ullage should be around 5%. This will be elaborated upon in a later section, but in essence, a reasonable ullage is still required for nitrous (although it is self-pressurizing) due to its vaporization rate. It takes a moderate amount of time for the nitrous to begin boiling and repressurizing once the engine begins to run, and during this time, the propellant tank is only being pressurized by the ullage space. If the ullage percentage is low, a slight expansion in the ullage volume would represent a disproportionately large relative increase in volume as compared to its increase if it were to occur mid-burn. Thus, this dramatic relative increase in volume causes a massive pressure drop in the opening seconds of an engine run if the initial ullage fraction is not sufficiently high.

The relation for isentropic expansion is

$$\frac{p_2}{p_1} = \left(\frac{V_1}{V_2}\right)^{\gamma} \tag{4.21}$$

where a subscript of 1 represents initial conditions and subscript of 2 represents final conditions. Since a burn time t_b was established in 1 to be around 5 seconds, a constant density ρ of 789 kg/m^3 and mass flow rate $dotm_f$ of 0.139 kg/s can be used to find that the initial volume occupied by ethanol is $[(0.139\ kg/s)(5\ sec)/(789\ kg/m^3)](1000\ m^3/L) = 0.881\ L$. The same procedure can be followed for nitrous and is found to be 3.59 L. Using the established ullage fraction of 2/3, it is apparent that the initial ullage volume for ethanol should be $V_1 = (0.881\ L)(3)(2/3) = 1.762\ L$ and thus the total tank volume is $V_{total} = V_2 = 0.881\ L + 1.762\ L = 2.643\ L$. Then, using Equation 4.21 and a γ value for N_2 gas of 1.40, an initial ethanol propellant tank pressure can be calculated, assuming the final ethanol tank pressure p_2 to be simply the chamber pressure P_c plus the system pressure drop Δp_{sys}:

$$(p_1)_f = \left[\frac{p_2}{(V_1/V_2)^{\gamma}}\right] = \left[\frac{1.5\ MPa + 509.2\ kPa}{(1.76\ L/2.643\ L)^{1.40}}\right] = 3544467\ Pa = 3.550\ MPa \approx 515\ psi$$

For nitrous, having a ullage of 5% and an initial liquid volume of 3.59 L, the ullage volume is $V_1 = [(0.05)(3.59\ L)]/(1-0.05) = 0.1889\ L$. The total tank volume is $V_{total} = V_2 = 3.59\ L + 0.1889\ L = 3.779\ L$. The initial volume is once again the chamber pressure plus the system pressure drop $p_2 = P_c + \Delta p_{sys} = 1.5\ MPa + 1.879\ MPa = 3.379\ MPa \approx 490\ psi$. However, the initial oxidizer tank pressure is not determined by Equation 4.21 since it is driven by the self-pressurization properties of nitrous oxide. Review of the behavior of nitrous oxide from a literature review (including [1]) concluded that the stable nitrous vapor pressure at 298 K is around 750 psi. This is a reasonable fit for the system since, as mentioned previously, the required final pressure is around 490 psi.

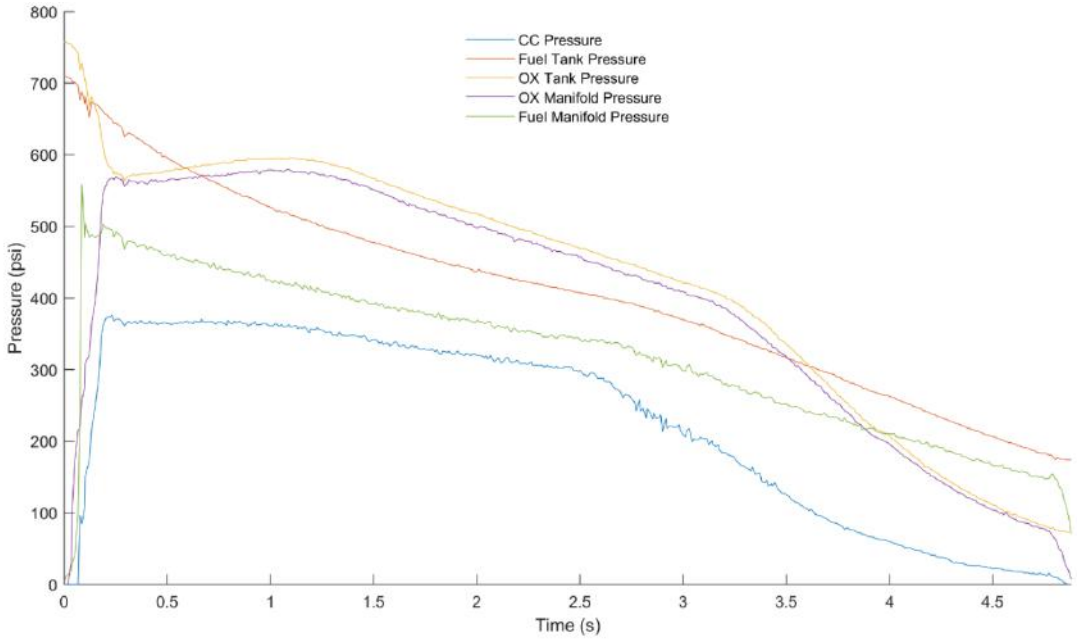

Figure 24: Empirical pressure profile of multiple components from a static engine test of MASA's Laika launch vehicle. Note the yellow line which begins at around 750 psi at 0 seconds, which represents the pressure readings from the oxidizer (nitrous) tank.

It can be seen from Figure 24 that the nitrous tank dropped from 750 psi to around 490 psi in around 3 seconds, albeit for completely different flow parameters. The steep drop in nitrous tank pressure, as mentioned before, can also be observed in the first few milliseconds in Figure 24.

However, with these broad ullage estimates and highly custom tank sizes, the previous tank calculations fail to account for manufacturing concerns and budget constraints. Fabricating custom tanks is not only out of the manufacturing scope of Project Caelus, but is also more expensive and more dangerous than if a commercial off-the-shelf (COTS) model was used instead. A scuba tank, the Metal Impact Aluminium 80 Cylinder from Dive Gear Express, was purchased due to its high safety factor (SF) pressure rating for 3000 psi, prerequisite hydrostatic safety tests, and compatibility with nitrous oxide. The actual volume of the cylinder is around 11.564 L. Using this cylinder for both propellants, the final volume p_2 becomes 11.564 L and the ullage volume p_1 is simply p_2 subtracted by the liquid volume. Using Equation 4.21 once again for ethanol gives

$$(p_1)_f = \left[\frac{p_2}{(V_1/V_2)^\gamma}\right] = \left[\frac{1.5\ MPa + 509.2\ kPa}{[(11.564\ L - 0.881\ L)/11.564\ L]^{1.40}}\right] = 2244936\ Pa = 2.245\ MPa \approx 326\ psi$$

The ullage volume for ethanol is simply $11.564\ L - 0.881\ L = 10.683\ L$, and the ullage percentage for ethanol is therefore $(11.564\ L - 0.881\ L)/(11.564\ L) = 92.4\%$.

For nitrous, although the inital and final pressures remain the same, the ullage volume is $V_1 = 11.564\ L - 3.59\ L = 7.974\ L$ and the ullage percentage is $7.974\ L/11.564\ L = 69.0\%$.

4.4 Plumbing System Procedural Design

Finally, with the plumbing system fully parameterized, the last step is determining the procedures in operating the system, more specific design subtleties in the P&ID, and safety precautions. There were

[2]These parameters are not final and are slightly adjusted later during system validation (see Section 6).

Piping System Main Parameters		
Name	Oxidizer (N_2O)	Fuel (C_2H_5OH)
Engine cycle	Pressure blowdown	
Pressurant gas species	Nitrous oxide	Nitrogen (N_2)
V_2, Final (total) tank volume	11.564 L	11.564 L
V_1, Initial (ullage) tank volume	7.974 L	10.683 L
V_{prop}, Initial liquid propellant volume	3.59 L	0.881 L
Ullage percentage	69.0%	92.4%
p_2, Final tank pressure	3.379 MPa (490 psi)	2.009 MPa (291 psi)
p_1, Initial tank pressure	5.171 MPa (750 psi)	2.245 MPa (326 psi)
Δp_{sys}, System pressure drop	1.879 MPa	509.2 kPa
Δp_{inj}, Injector pressure drop	375 kPa	375 kPa
Δp_{val}, Valve pressure drop	1.460 MPa	130.6 kPa
Δp_{ext}, Head/extraneous pressure drop	43.8 kPa	3.61 kPa
d, Pipe diameter	12.7 mm	

Table 8: Summary of main piping system parameters.[2]

several overarching design considerations, but perhaps the most important outlined that all pressurization and post-pressurization actions must be done remotely. This is so that no ground operators would need to approach a pressurized system, which would almost certainly be a safety hazard. Practically, this means that a ground electronics system would be required to operate during engine tests. Another consideration was that the system must be able to vent pressure and drain propellant both remotely and manually. Finally, the system must have adequate redundancy where it is necessary to ensure safety. Figure 21 displays the full P&ID, and it is displayed again below for the convenience of the reader. The following subsections will go into detail on different aspects of the plumbing system. It is important to note that the ethanol fill and pressurization use the same inlet in order to save costs and avoid purchasing unnecessary hardware.

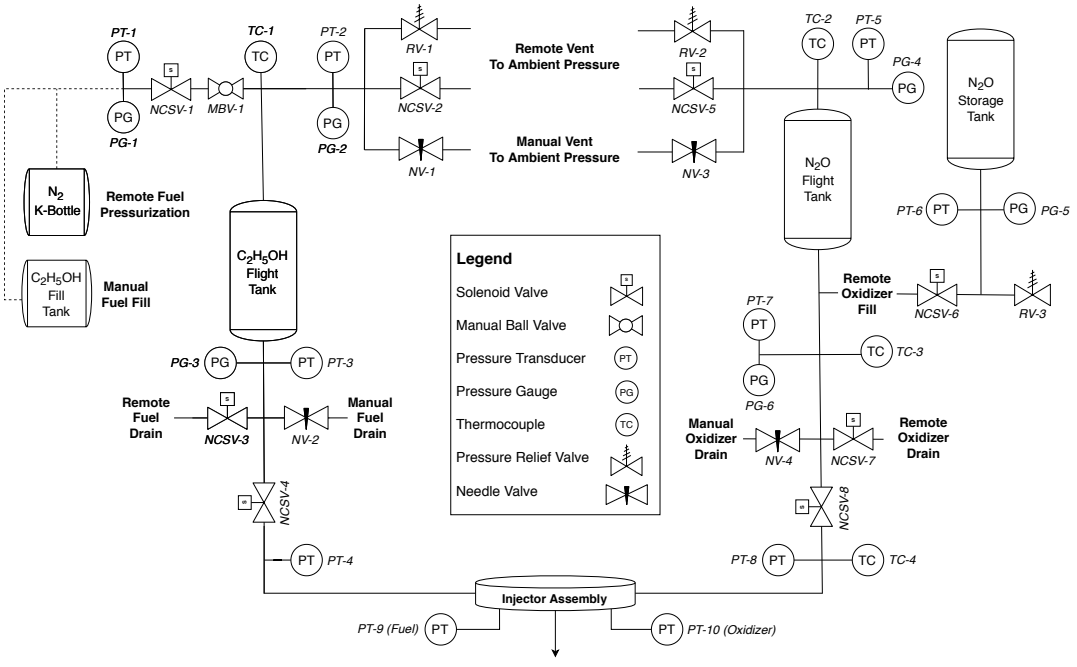

Figure 25: Full system piping and instrumentation diagram (P&ID).

4.4.1 Ethanol Fill System

A gravity fill, a method in which all work is done by gravity (not pressure) to transfer the propellant from the fill tank to the flight tank, was chosen for ethanol as it avoids the use of expensive pumps or

additional pressurization equipment. First, ethanol will be poured manually into the propellant tank since it is nontoxic and non-cryogenic. During this time, both MBV-1 and NCSV-1 will be open to allow to ethanol to begin to fill the flight tank. Once this is complete, MBV-1 and NCSV-1 will be closed and the nitrogen K-bottle (pressurant storage tank) will be attached at this port to the rest of the piping system. This is done to minimize the number of possible failure points while ground team members are still in the vicinity of the system. This section of the system is displayed in Figure 26.

4.4.2 Ethanol Nitrogen Blowdown Pressurization System

Pressure blowdown, as mentioned previously, was chosen as the method of pressurization due to its simplicity, along with a few other benefits that will be discussed here. One such benefit is that during launch, the utilization of pressure blowdown would negate the need for a completely seperate pressurant tank (the pressurant tank technically remains on the ground, which detaches from the vehicle via quick disconnects and pneumatic actuators) and therefore significantly lower the dry mass of the rocket. Additionally, the large ullage percentage of the propellant run tank and short engine burn time dismisses the potential benefits of a pressure-regulated system, as a steady chamber pressure and thrust is not of concern. The nitrogen gas used for the pressure blowdown will initially be stored in a K-bottle at around 2,000 psi.

NCSV-1 (normally-closed solenoid valve) will be remote-operated for control of pressurant flow, while MBV-1 is the isolation valve to ensure that pressurant is not unintentionally released while ground operators are near the test stand. The solenoid valve was chosen to be normally-closed so that in the event of power loss to the test stand, the flight tank and K-bottle will be isolated to prevent further cross-feed or pressurization. PT-1 and PG-1 will provide data on the pressure of the pressurant tank during pressurization. PG-1, along with other pressure gauges, are routed to a common panel where it is captured through a camera so that operators can confirm pressure transducer readings in real-time without approaching the test stand. Once ethanol has been filled, the nitrogen K-bottle has been properly connected, and all other checks are completed, the nitrogen K-bottle valve will be opened and PT-1 and PG-1 will start reading pressure data. Finally, MBV-1 will be opened and all personnel will evacuate the test stand area and return to (most likely) a safety bunker. NCSV-1 will then be opened remotely, allowing nitrogen from the K-bottle to flow into the tank until the tank is pressurized to the proper pressure. This is once again illustrated in Figure 26.

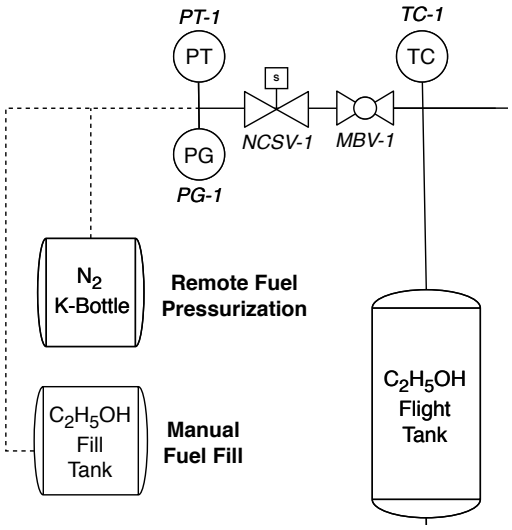

Figure 26: The ethanol fill and nitrogen blowdown pressurization system.

4.4.3 Ethanol Pressure Vent System

The ethanol pressure vent system is the fail-safe system responsible for reacting to undesirable or dangerous changes to the system state. Its main function is to relieve pressure from the ethanol tank, whether that be manually, remotely, or automatically. The two most prevalent cases are: 1) in the event of an overpressurization of the flight tank or overall system that exceeds safety margins, or 2) in

the event of a catastrophic engine or MPV failure that requires a decrease in ethanol flow rate. The system consists of three main valves. The first of these is RV-1, a pressure relief valve, which will be set to automatically open if tank pressure exceeds 600 psi, which is almost 100% greater than would be nominally expected (although the tank is rated for 3000 psi). The second valve is NCSV-2, a solenoid valve, which can be remotely opened and closed at the content of the operator. The flight software team has developed two separate actions available to NCSV-2 in order to refine the control of the pressure inside the ethanol tank: 1) a "pulse", which is a pre-programmed opening, time delay, then closing of NCSV-2 for small and incremental pressure vents, and 2) a "toggle", which simply switches the solenoid state to either closed or open. NCSV-2 is used generally when fine pressure adjustments are required, or in the case of a failure with RV-1, a full system abort. NCSV-2 would logically be best suited as a normally-open solenoid so that it can vent pressure even in the case of power loss, but was chosen to be normally-closed purely for financial reasons. Finally, NV-1, a needle valve, will be used for any manual draining or venting purposes as a last resort or when the system is only barely pressurized. It can also be used to slowly ease tank pressure once the solenoids and pressure relief valves have already adequately dumped pressure for engineers to safely approach the test stand. Lastly, PT-2 and PG-2 both serve the purpose of monitoring and recording the ethanol pressure during operation and flight. TC-1, a thermocouple, is not mission-critical but serves to confirm data from simulated tank models. This system implements redundancy (RV-1 and NCSV-2) by ensuring that there is always a back-up to relieve tank pressure when it is necessary, even if a valve fails. This system is displayed in Figure 27.

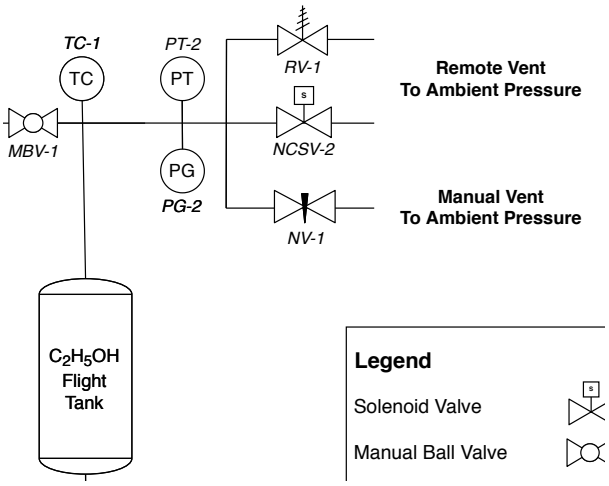

Figure 27: The ethanol vent system.

4.4.4 Ethanol Main Propellant Line and Drain System

The main propellant line is the flow path of the propellant between the flight tank and the injector assembly. Immediately downstream of the flight tank, the propellant first encounters the two pressure sensors. PT-4 and PG-4 monitor the pressure of liquid ethanol exiting the propellant tank. Since the distance between the exit of the ethanol tank and the MPV is small, the readings from PT-4 and PG-4 can be regarded as simply the inlet pressure to the MPV and can be used during post-processing to calculate the flow coefficient (C_v) of the MPV. Next, the fluid encounters the drain system, which comprises of two valves, NCSV-3 and NV-2. The drainage of liquid propellant is necessary to clear the propellant lines of residual propellant after an engine run, or when redirecting propellant out of the system is necessary during an emergency. The first valve is NCSV-3, a remotely-operated solenoid, which will be used for the majority of drainage cases (particularly in the case of a system abort). The second valve is NV-2, a manually-operated needle valve, which will serve as a secondary method of draining propellant when the propellant pressure has been adequately relieved or when manual operation is necessary. Downstream of the drain system is NCSV-4, which is the main propellant valve. The MPV's primary purpose is to either prevent or allow flow between the fuel tank and the engine. This is to prevent further propellant for combustion from reaching the engine in the event of a catastrophic engine failure. The MPV can be remotely actuated from either the ground station or from the on-board flight computer. Since the MPV is the only major obstruction of flow in both propellant towers, care is taken to accurately measure its flow coefficient. This is the primary purpose of PT-4, as it measures both the pressure immediately following

the MPV and gives an accurate estimate of the pressure preceding the injector assembly. Lastly, PT-9 measures the pressure inside the injector manifold, just before it is injected through the injector plate and into the combustion chamber. This system is displayed in Figure 28.

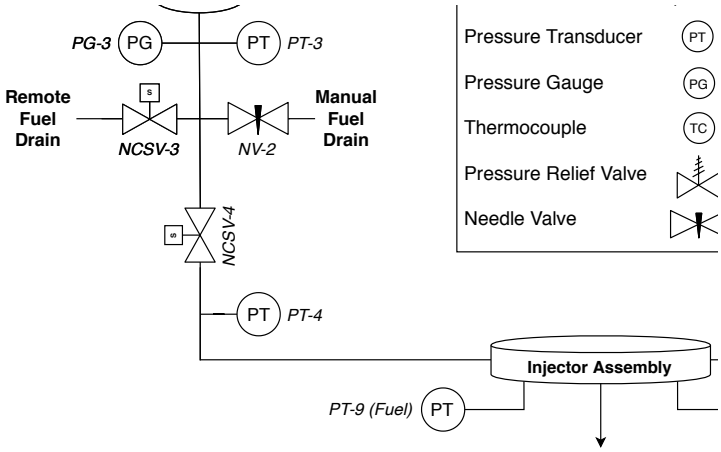

Figure 28: The ethanol main propellant line and drain system.

4.4.5 Nitrous Oxide System

Although the properties of nitrous vastly differ from that of ethanol, the design of its plumbing system is largely the same, as seen from Figure 21. In this section, only the significant differences from the ethanol tower will be discussed. Similarities in the two systems can be inferred to be chosen for the same reason.

The most obvious difference between the two propellant towers involves their fill and pressurization systems. Since nitrous is self-pressurizing and ethanol is pressurized prior to any nitrous entering the system, the procedure for loading nitrous is completely remote. When the nitrous storage tank is first connected to the system, NCSV-6 is closed to prevent any pressurization. Once ground operators have cleared the area and the ethanol tower has completed its pressurization procedure, NCSV-6 is opened to allow liquid nitrous oxide to gravity fill into the propellant tank. As the nitrous fills, RV-3 (a relief valve) may open at any time as a redundancy against overpressurization. The nitrous storage tank is placed physically higher than the nitrous flight tank to achieve this. All other valves in the nitrous tower are closed at this time. Once a predetermined amount of liquid nitrous has been expelled from the storage tank, NCSV-6 is closed and time is allowed to elapse until the vapor pressure inside the flight tank has reached equilibrium. In addition to using PT-5 and PG-4 to monitoring nitrous pressure, TC-2 is critical to determining the state of the nitrous due to N_2O's behavioral sensitivity to temperature. Note how additional thermocouples are also placed along the nitrous main propellant line for this reason. Once the operator is satisfied with the liquid volume and nitrous pressure, NCSV-8 (the nitrous MPV) can be opened along with NCSV-4 (the ethanol MPV) to begin engine operation.

5 Test Stand Design

In the development of rocket propulsion systems, it is often necessary to test individual systems on the ground before attempting a flight. These tests are typically classified in two categories: a cold flow test, where the plumbing and instrumentation systems are the focus of the test (no ignition for combustion occurs), and a static hot fire test, where the full system can be tested in flight conditions except for the forces on the vehicle. For the purposes of safety and an iterative approach to testing, the cold flow test is further broken into three separate tests. First, a hydrostatic test, where the system is simply filled and pressurized with water, is conducted to test the structural integrity and pressure rating of the system without involving any controlling software. Secondly, an ethanol cold flow will we conducted to test the ethanol propellant tower in isolation from the nitrous tower. Since water has properties that are very similar to ethanol, it will be substituted for ethanol on the first cold flow test to save costs and eliminate a fire hazard. In addition, since nitrous is significantly more hazardous than ethanol, it is

Figure 29: The ethanol propellant tower test stand. The cinder block assembly and K-bottle are also shown.

Figure 30: The full ethanol propellant tower test stand, with a linear rail system for housing the engine.

expected that most software and procedural tests will be conducted on the ethanol cold flow test. More specifically, the ethanol cold flow test contains objectives that include: empirically verifying theoretical predictions for system behavior (such as pressure drops, C_v values, injector spray pattern), testing software functionality (such as abort sequences, pre-stage, remote valve operations, and data acquisition), and most importantly, executing procedural tests, such as procedures for system assembly, part-cleaning, leak-checking, filling, pressurization, draining, manual overrides, and all abort cases. Finally, the last cold flow involves testing the nitrous tower. Since nitrous is a strong oxidizer, additional safety precautions will be taken. In addition, due to its properties, different fill and pressurization procedures will be tested and finalized. However, it is expected that this test will exhibit minimal risks and failures since the bulk of system functionality would have already been tested through the ethanol cold flow test.

The following section discusses the design for the test stand in which all cold flow tests are expected to take place. Due to a limited budget, efforts were made to increase the adaptability for this cold flow test stand to eventually be used for a static engine hot fire test. This design is presented in the context of an ethanol cold flow test.

5.1 Ethanol Cold Flow

The ethanol cold flow will be executed at two different states: at full pressure or at scaled pressure. This is due to the fact that the overall system pressure drop will be greater than that expected during actual engine operation, since there is no back-pressure from the combustion chamber. Both of these methods will provide different but nonetheless valuable information about the system and provide procedural practice to progress towards a static hot fire of the engine.

A full pressure cold flow test involves pressurizing the tank its nominal pressure during a hot fire (full pressure). This is to test the pressure rating of all parts of the system, including valves, tubing connections, and sensors, and to verify that these parts operate as expected whilst under this pressure. Furthermore, a full pressure cold flow is best for testing abort sequences since the pressure gradient with ambient pressure is unchanged for the venting and draining system. The disadvantage of a full pressure test is that since the system pressure differential to the combustion chamber is higher than nominal, the flow behavior throughout the system is not accurate of a hot fire (flow rates and pressure drops are higher). To remedy this, a scaled pressure test can be conducted.

A scaled pressure cold flow models the flow behavior throughout the system most accurately by setting the pressure differential between the tank and chamber equal to the actual differential expected in the static fire. This is done by lowering the initial pressure inside the ethanol flight tank to counteract the ambient pressure present in the combustion chamber. This allows accurate measurements of system and part C_v values, as well as mass flow rates and tank depletion profiles over time.

To accomplish these testing tasks, the plumbing system detailed in the system P&ID (Figure 21) must be fully constructed as a functional and modular test stand, along with a separate injector and engine housing mechanism to withstand the structural load and measure thrust in a static hot fire. The following subsections will detail these two major components of the test stand.

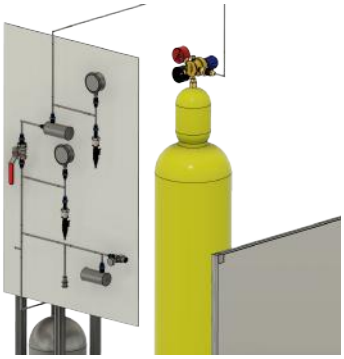

Figure 31: The upper plate (upstream of flight tank).

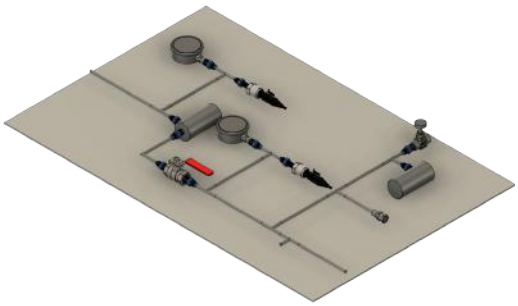

Figure 32: Detailed view of the upper plate.

Figure 33: The lower plate (downstream of flight tank).

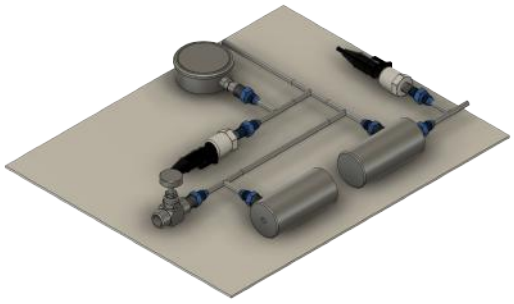

Figure 34: Detailed view of the lower plate.

5.2 Tank Stand and Plumbing Circuit

The tank stand accommodated the ethanol flight tank, nitrogen K-bottle for pressurization, and all its corresponding plumbing circuits, including the pressurization system and all plumbing components downstream of the flight tank (up to the injector assembly). It is displayed in Figures 29 and 30. The design for this test stand included a frame of aluminium 80/20 extrusions that acted as the primary structural component for holding the ethanol flight tank. Aluminium 80/20 extrusions were chosen due to their availability and since they could easily be rearranged and fastened without the need for welding. A cinder block assembly was created to act as an elevated stand for the temporary nitrogen K-bottle. The plumbing system was separated and organized into two plates, the upper plate and lower plate. The upper plate housed the plumbing for the vent and pressurization systems (upstream of the flight tank), while the lower plate housed the drain system and MPV (downstream of the flight tank). These plates were 1/8" thick steel or aluminium plates in which the plumbing system was bolted to. The plates themselves could be bolted on the exterior of the 80/20 aluminium frame, which houses the ethanol tank. The use of plates will allow for all plumbing to be visible and easily accessible for manual operations, such as reading pressure gauge data and turning manual valves. The plate will additionally serve as a support structure for the piping. These plates are shown in detail in Figures 31, 32, 33, and 34.

Additional considerations were made when designing these plates in 3D space. Perhaps most importantly, they were made to be as compact as possible to reduce the total material needed. Pressure relief valves were also designed to point away from any other mounted instrumentation. Care was taken to ensure these plates were secured properly and at strong points on the frame so that if the pressure relief valves produced significant thrust due to rapid depressurization, the damage would be minimal. All major components including valves, joints, gauges, sensors, and AN to NPT adaptors are included and shown in Figures 32 and 34.

Because the nitrogen K-bottle connects to the plumbing from a tube located at the top of the upper plate, the cinder block arrangement was used to elevate the K-bottle to reducing the amount of tubing needed to reach that location. This method of reducing external tubing was determined to be easier and more efficient than other methods, such as fully mounting the K-bottle above the upper plumbing plate, which would have required more materials and support to accommodate the additional weight. Additionally, the availability, ease of construction, and flexibility of the cinder block arrangement made

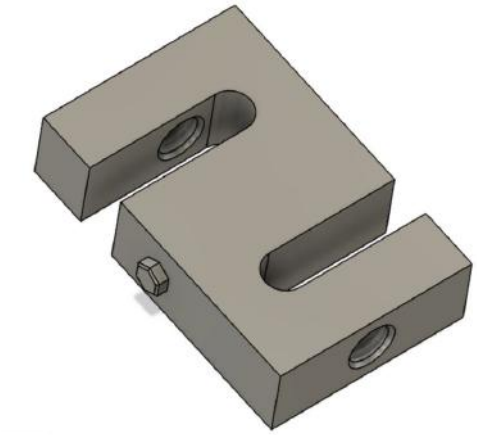

Figure 35: S load cell.

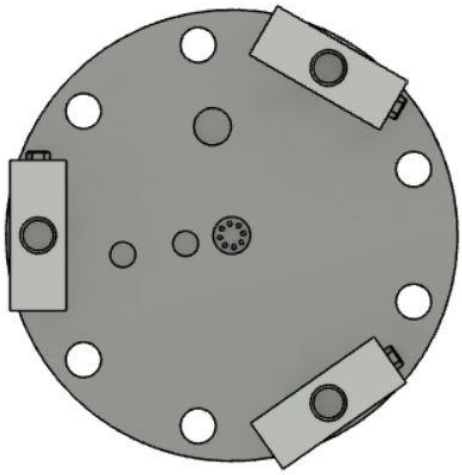

Figure 36: Three load cell mounting.

it an appealing choice. The system test stand (excluding the engine mount) can be seen in Figure 29.

5.3 Engine and Injector

A mounting utilizing load cells was designed to secure the engine to the test stand and allow for thrust measurements of the engine during a hot fire. The mounting uses three load cells in a triangular formation that will allow for more accurate readings and increased stability. The s-type load cell was selected for both its price and range or readings. The load cell can be seen in Figure 35. The formation of the three load cells can be seen in Figure 36 and 37. The presence of screw holes on both ends of the load cell makes them suitable to mount the engine directly to the test stand. Calculations were performed to ensure that the screws in the the load cells would be capable of holding up the engine. This mount can be seen in Figure 38.

Although firing the engine horizontally introduces some potential hazards in the engine startup transients, such as propellant pooling, it was determined that these drawbacks are outweighed by the simple and cost-effective nature of a horizontal test stand. The forces produced by the engine can simply be counteracted by placing a heavy object ahead of the engine (as opposed to a vertical stand, which would require more complex structures) and fuel pooling can be addressed by adequately testing the ignitor system. The load cell is mounted horizontally onto the main blast shield plate, which is the large square plate that separates the engine from the plumbing system. There are three connection holes in the blast shield: one for the fuel line, one for the oxidizer line, and one to allow electrical connections to pass through the plate. During a cold flow, only the injector assembly would be mounted with the load cells.

6 System Validation and Simulation

The final step in the design of the Aphlex 1B system was to generate the expected engine profiles (thrust, chamber pressure, mass flow rates, O/F ratio) during static hot fires through a numerical simulation and therefore validate the system with the generated data. Due to the complex and dynamic nature of both nitrous oxide and pressure blowdown systems, a MATLAB script utilizing time-step-based integration to model incremental changes in the system state was used. The bulk of the MATLAB script was based off Nick Gloria's (Stanford Space Initiative) propulsion simulation code, which can be found here `https://github.com/ngloria1/PropSim`. This branch was forked so that slight modifications to the code could be made (discussed below), which can be found here `https://github.com/JayChen35/PropSim`.

PropSim works, on a basic level, by modelling and storing all state variables (such as the mass and volume inside each tank, pressures at critical points, temperatures, etc.) in a state vector. A small time differential dt is chosen to calculate a slight change in the system state given a small change in time. For

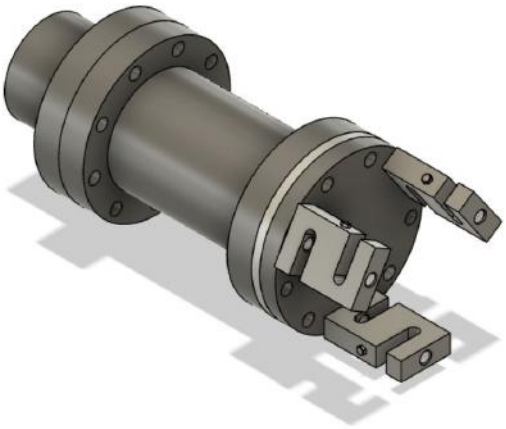

Figure 37: A side view of the three load cell mounting.

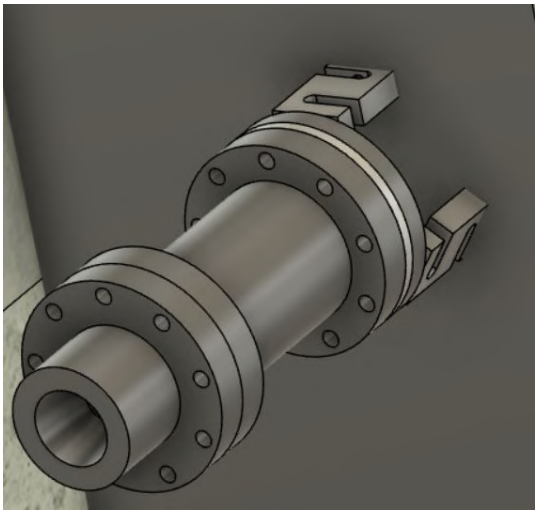

Figure 38: The load cell mounting on the test stand.

each time step calculation, the mass flow rates of the oxidizer and fuel tank (given the temperatures and pressures of the previous state vector) are first computed, given a system C_dA (a pressure drop term and flow rate term similar to C_v). In Nick Gloria's code, the C_dA value is only driven by the discharge coefficient the total orifice area of the injector (see Table 4). The modified version of the code accounts for other losses in pressure, such as through an MPV, by summing additional C_dA terms. C_dA is defined as

$$C_dA = \frac{\dot{m}}{\sqrt{2\rho\Delta p}} \tag{6.1}$$

where the term $sqrt2\rho\Delta p$ is also known as *mass flux*, denoted as G. It is seen here that C_dA is simply the product of the discharge coefficient C_d and the cross-sectional area A of the flow. C_v is defined in Equation 4.17. To relate CdA to C_v, some algebra is required by setting Q to $\dot{m} \times \rho$. The result is

$$C_dA = C_v \left(\frac{1}{\sqrt{2/\rho_{H2O}}} \right) \tag{6.2}$$

However, since the unit for C_v is imperial ($gal/\sqrt{psi}$), a conversion factor is required. Using this conversion factor, Equation 6.3 relates C_dA to C_v, with C_dA in m/s:

$$C_dA = 7.598 \times 10^{-7} \left(\frac{C_v}{\sqrt{2/\rho_{H2O}}} \right) \tag{6.3}$$

To incorporate multiple C_dA values of components in series (such as the MPV and injector plate), a summation law similar to that of summing resistors in a parallel circuit, is used:

$$C_dA_{eff} = \left(\sqrt{\frac{1}{(C_dA_1)^2} + \frac{1}{(C_dA_2)^2}} \right)^{-1} \tag{6.4}$$

where C_dA_{eff} is the effective system C_dA. Equations 6.3 and 6.4 were implemented in the modified code to account for the injector and MPV pressure drops. Using C_dA_{eff}, mass flux, and Equation 6.1, new mass flow rates for both propellants are computed. This mass flow rate is retained in a system state differential vector, the state dot vector, where it is later integrated using *ode15s* (Euler integration method) to determine the new system state vector.

Following this mass flow rate calculation, a function modeling nitrous is executed to determine the new equilibrium state for the nitrous propellant tank. This function assumes two-phase nitrous flow and models its behavior using the Homogeneous Equilibrium Model (HEM), which is outlined in [6]. Propellant tank dynamics follow the van der Waal's equation for gases, and assume thermal equilibrium between the gas and liquid inside the tank. Finally, combustion and expansion through the nozzle is modelled via quasi-1D isentropic flow, as outlined in Section 3.1. The state vectors at each dt are recorded and plotted once the simulation is terminated.

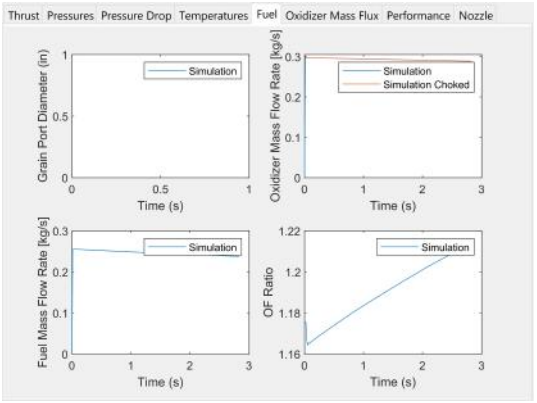

Figure 39: Thrust output of the simulation code with both MPVs modelled.

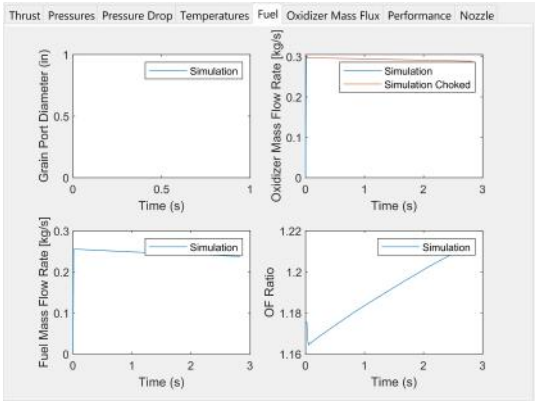

Figure 40: Propellant mass flow rate plots of the simulation code with both MPVs modelled.

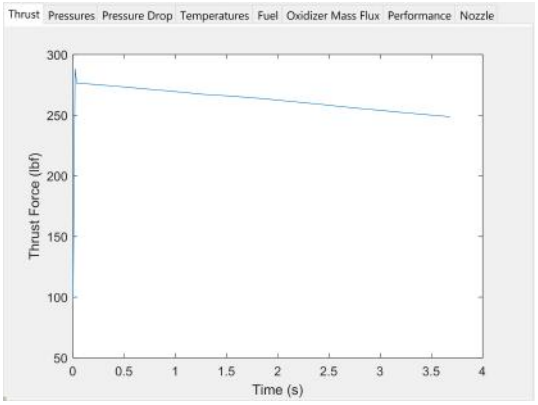

Figure 41: Thrust output of the simulation code with the N_2O MPV removed.

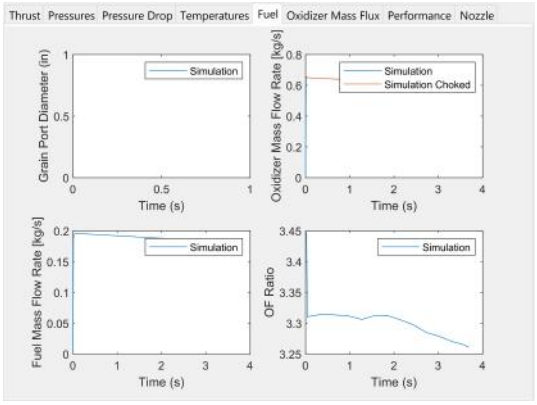

Figure 42: Propellant mass flow rate plots of the simulation code with the N_2O MPV removed.

Figure 39 shows the thrust profile of the simulated engine burn with both MPVs modelled. It is clear that the engine is severely short of its design thrust, and Figure 40 reveals the cause: the oxidizer MPV severely restricts the $\dot{m}_o$ to the engine, causing a skewed O/F ratio, thus lowering combustion pressure and temperature.

Removing the oxidizer MPV shows a promising engine profile, as shown in Figures 41 and 42. Although removing the nitrous MPV can be seen as a safety hazard, the practice is not uncommon and system adjustments can be made to counteract its drawbacks. Many hybrid propulsion systems utilize burst disks instead of an MPV to allow flow to begin through the propellant lines once a threshold pressure has been reached. In addition, since combustion requires both propellants to be present, the ethanol MPV can alone be used to halt combustion. The nitrous drain and vent systems can also assist in preventing N_2O from entering the chamber.

Apart from removing the nitrous MPV as a method of increasing $\dot{m}_o$, there are three alternatives, although none are particularly desirable. First, a larger and higher C_v solenoid can be purchased. This is the obvious choice but will inevitably drive up costs. Second, another type of valve can be purchased or made, such as a ball valve. This is not desirable since designing and testing a reliable actuation system for a ball valve can be meticulous and prone to error. The general philosophy is to rely on COTS components, but COTS actuated ball valves cost significantly more than the current MPV. Finally, increasing upstream pressure could also increase $\dot{m}_o$. However, this is brute-force method that not only causes the system to be less safe, but also unnecessarily increases the propellant tank (and vehicle) dry mass. At this time, no decision has been made to determine the best course of action, although it is expected that any changes made to the design should come easily, due to the modularity of the system.

It can also be noted that the system burn duration (as seen in Figures 41 and 42) is shorter than expected. Upon closer inspection, it can be deduced that this is due to a higher fuel mass flow rate, caused by a sub-optimal O/F ratio (and thus, sub-optimal chamber pressure). To compensate for this, parameters in Table 8 are adjusted according to the updated mass flow rate from Figure 42. It is

estimated that $\dot{m}_f = 0.2\ kg/s$ and $\dot{m}_f = 0.6\ kg/s$. Thus, the new fuel mass and volume are $(m_f)_0 = (0.2\ kg/s)(5\ s) = 1.0\ kg$ and $(V_f)_0 = (1.0\ kg/s)/(789\ kg/m^3)(1000\ L/m^3) = 1.267\ L$. For nitrous: $(m_o)_0 = (0.6\ kg/s)(5\ s) = 3.0\ kg$ and $(V_f)_0 = (3.0\ kg/s)/(772.25\ kg/m^3)(1000\ L/m^3) = 3.885\ L$.

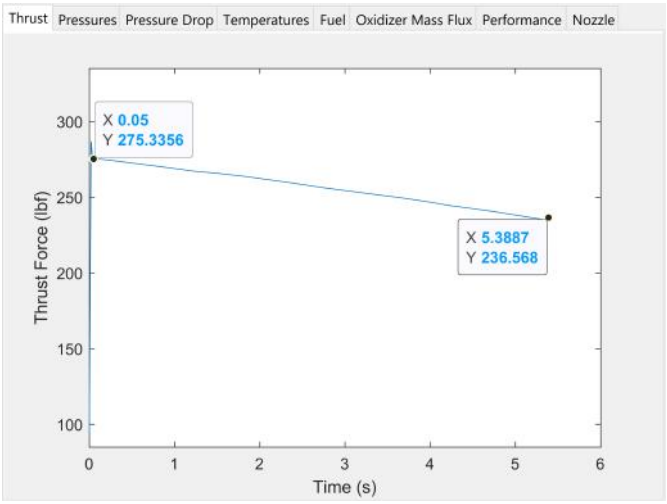

Figure 43: Thrust output of the simulation code without an N_2O MPV and with the updated initial masses.

Figures 44 through 49 how the detailed system profiles with the updated propellant masses. Some additional information is provided here:

```
% >> SimulateLiquidMod.m
% Initial oxidizer mass: 4.46 kg
% Pressurant Mass: 0.267 kg
% Impulse: 6.14 kN*s
% Oxidizer Mass Spent: 3.29 kg          Oxidizer Mass Remaining: 1.18 kg
% Fuel Mass Spent: 1.00 kg              Fuel Mass Remaining: 0.00 kg
% OF ratio: 3.29
% Isp: 146.0 s          C*: 1149 m/s          C_f: 1.25
```

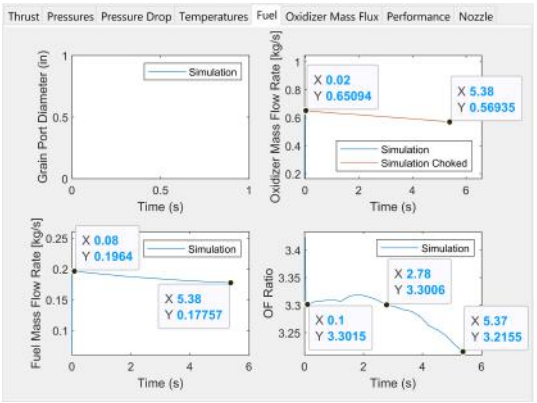

Figure 44: Mass flow rate plots without an N_2O MPV and with the updated initial masses.

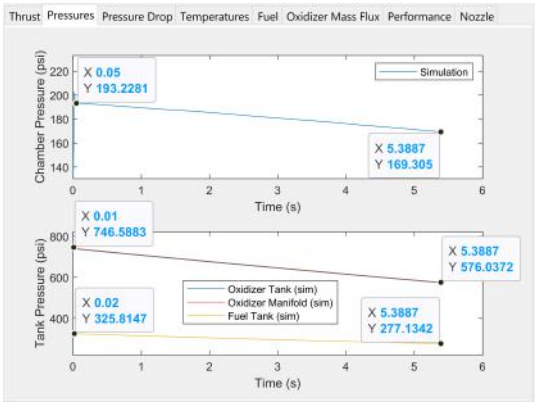

Figure 45: Chamber and tank pressure profiles without an N_2O MPV and with the updated initial masses.

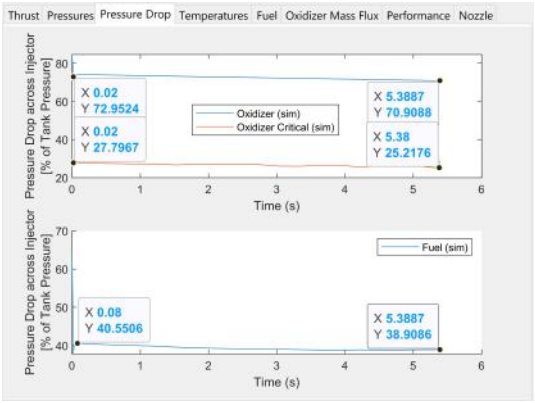

Figure 46: Fuel and oxidizer injector Δp profiles without an N_2O MPV and with the updated initial masses.

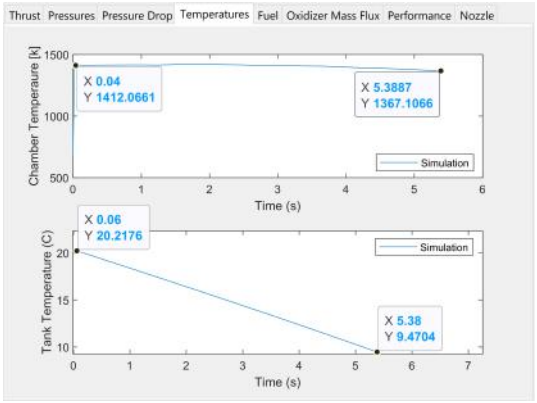

Figure 47: Chamber and tank temperature plots without an N_2O MPV and with the updated initial masses.

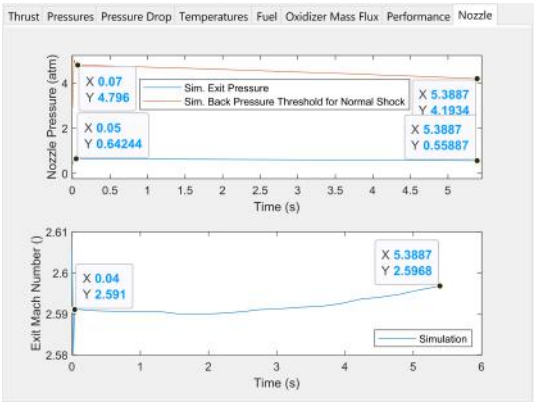

Figure 48: Nozzle characteristic profiles without an N_2O MPV and with the updated initial masses.

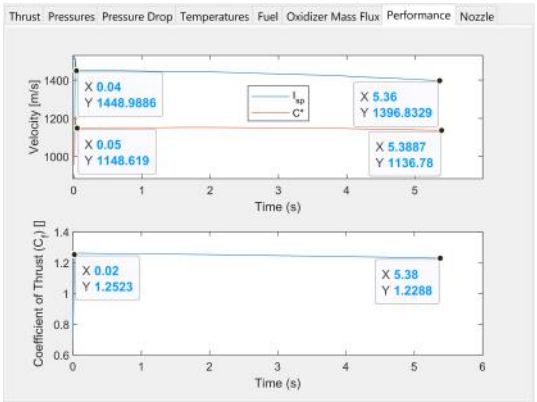

Figure 49: System performance profiles without an N_2O MPV and with the updated initial masses.

7 Parts and Budget

7.1 Valves

The valves were selected based on criteria of material compatibility with nitrous oxide, flow coefficient (Cv), price, maximum pressure, and pipe size. The optimum available material for nitrous compatibility is stainless steel 316 (Swagelok citation), but for the first three valves, brass was chosen as the body material to minimize costs. Additionally, although the propellant tower pipes have AN fittings, essentially all available parts had national pipe thread (NPT) fittings; this necessitated numerous AN to NPT adapters. The prohibitively high cost of large solenoids with a high maximum pressure rating led us to choose Asco's 1/4"NPT solenoid, although it requires AC to DC conversion. For both the pressure relief valve and needle valve, Generant was chosen since it offered the options we needed. DiscoverValve offered a high-Cv ball valve that was also low cost and made of stainless steel, so it was selected as well.

Valve Type	Max Pressure	Cv	Manufacturer	Part Number
Solenoid	1500 psi	1.5	Asco	8223G025
Pressure Relief	1000 psi		Generant/Rego	HPRV-500-B-B-600
Full-Port Ball	1000 psi	16	DiscoverValve	101099
Needle	5000 psi	0-0.4	Generant	3000-10B

7.2 Sensors

Sensor Type	Max Pressure	Outlet	Manufacturer	Part Number
Pressure Gauge	1000 psi	1/4” MNPT	UPE Group	N/A
Pressure Transducer	1000 psi	1/8” MNPT	Ebay	N/A
Thermocouple		1/4” MNPT	Omega	N/A

7.3 Fittings

To minimize costs and maximize the chances of finding a suitable direct transition, the material for fittings and adapters was anodized, aircraft-grade aluminum, which is far more resistant to nitrous oxide than less specialized variants. The types of adapters were chosen to suit both the 1/2” pipe in 08AN and the parts with ports of 1/2”, 1/4”, and 1/8” in NPT. Additional parts were selected to fulfill special transitions. The 1/8”NPT pressure transducer posed a special problem for adapters, so its transition was integrated with the pressure gauge’s transition, allowing a special 1/2” part with a 1/8” top port to be used. Because some parts had male connections and others had female connections, separate MNPT and FNPT adapters were needed. In the instance where a pressure transducer did not have an accompanying pressure gauge, a 08AN piece with male connections on both sides was used to keep the 08AN with 1/8”NPT port piece inline with the main pipe segment.

Fitting Type	Manufacturer	Part Number
T-Joint	Jegs	555-110233
1/2” AN to 1/2” NPT	Jegs	555-110109
1/2” AN to 1/4” MNPT	Jegs	555-110105
1/2” AN with 1/8” NPT Port	Jegs	555-110527
1/2” AN Male Connector	Evil Energy	CS00581AN8BK-2
1/2” AN to 1/4” FNPT	AutoBbox	WAN895-4D-08-blk

7.4 Tools

Tool	Manufacturer	Part Number
Tube Cutter	Ridgid	N/A
Tube Deburrer	Ridgid	N/A
Tube Bender	Imperial	N/A
Tube Flarer	Ridgid	N/A
Tube Straightener		N/A

7.5 Other Parts

Part	Max Pressure	Function	Manufacturer	Info	Part Number
Nitrogen	N/A	Pressurization	Praxair	Rental	N/A
Regulator		Pressure Regulation			N/A
Tubing	1200 psi	N/A	McMaster	6’, 0.035” thick	N/A
Stainless Steel	42000 psi	Injector Material			N/A

7.6 Budget

Part	Quantity	Unit Cost	Total Cost
Solenoid Valve	4	319.00	1276.00
Pressure Relief Valve	1	65.00	65.00
Ball Valve	1	22.71	22.71
Needle Valve	2	40.00	80.00
Pressure Gauge	3	14.50	43.50
Pressure Transducer	4	20.00	80.00
Thermocouple	1	00.00	00.00
T-Joint	7	11.11	77.77
1/2" AN to 1/2" NPT	6	3.59	21.54
1/2" AN to 1/4" NPT	2	5.12	10.24
1/2" AN with 1/8" NPT Port	6	9.40	56.40
1/2" AN Male Connector	1	8.99	8.99
1/2" AN to 1/4" FNPT	6	9.49	56.94
Tube Cutter	1	37.73	37.73
Tube Deburrer	1	37.95	37.95
Tube Bender	1	45.00	45.00
Tube Flarer	1	145.00	145.00
Tube Straightener	1	128.00	128.00
Nitrogen	1	20.00	20.00
Regulator	1	100.00	100.00
Tubing	5	38.25	191.25
Stainless Steel	1	25.00	25.00
Total	N/A	N/A	2,569.02

References

[1] Tomasz Palacz. "Nitrous Oxide Application for Low-Thrust and Low-Cost Liquid Rocket Engine". In: *7th European Conference for Aeronautics and Space Sciences* (July 2017).

[2] GVR Rao. "Exhaust Nozzle Contour for Optimum Thrust". In: *Jet Propulsion Archive* 28.6 (1958).

[3] George P. Sutton and Oscar Biblarz. *Rocket Propulsion Elements, 9th Edition*. Wiley, Dec. 2016.

[4] Travis S. Taylor. *Introduction to Rocket Science and Engineering*. CRC Press, 2009.

[5] Frank M. White. *Fluid Mechanics*. Fourth. McGraw-Hill Series in Mechanical Engineering. McGraw-Hill, Dec. 1998.

[6] Jonah E. Zimmerman et al. "Review and Evaluation of Models forSelf-Pressurizing Propellant Tank Dynamics". In: *49th AIAA/ASME/SAE/ASEE Joint Propulsion Conference* (Aug. 2013).